Received: 2 November 2024 | Revised: 16 February 2025 | Accepted: 22 February 2025

DOI: 10.1002/esp.70035

RESEARCH ARTICLE

ESPL WILEY

The impact of river capture on fluvial terraces and bedrock incision

Sean F. Gallen[1] | Karl W. Wegmann[2,3]

[1]Department of Geoscience, Colorado State University, Fort Collins, Colorado, USA

[2]Department of Marine, Earth and Atmospheric Sciences, North Carolina State University, Raleigh, North Carolina, USA

[3]Center for Geospatial Analytics, North Carolina State University, Raleigh, North Carolina, USA

Correspondence
Sean F. Gallen, Department of Geoscience, Colorado State University, Fort Collins, CO, USA.
Email: sean.gallen@colostate.edu

Funding information
National Science Foundation, Grant/Award Number: 2041910; American Chemical Society Petroleum Research Fund, Grant/Award Number: 50792-DNI8; Geological Society of America, Grant/Award Number: 9596-11; Sigma Xi; NSF-Geomorphology and Land-use Dynamics, Grant/Award Number: 2139894

Abstract

River terraces are commonly used to infer climate and tectonic histories. Yet, it is increasingly recognised that other processes, such as river capture, can affect river terrace genesis and incision rates and patterns. In this study, we conduct a field-based investigation of river terrace sequences along the Kolokithas and Varitis Rivers in central Crete, Greece, that share a confluence and preserve geomorphic evidence for the recent capture of the Kolokithas headwaters by the Varitis. We use digital topographic analysis, mapping, and optically stimulated luminescence (OSL) geochronology to quantify the river terrace and bedrock incision response to river capture. Topographic analysis indicates the Varitis captured ~30 km^2 of drainage area from the Kolokithas. We find differences in terrace characteristics, number of terraces, and incision rates and patterns on the adjacent valleys. The Kolokithas has four terrace levels, and the Varitis has five. All terraces are strath terraces, except for the oldest on the Kolokithas, a ~8 m thick fill terrace that starkly contrasts the time-equivalent ~1–2 m thick strath terrace on the Varitis. Relative and absolute age control suggests three Pleistocene terraces were emplaced during cooler climate intervals, and two Holocene terraces are perhaps because of anthropogenic disturbances. The incision patterns differ on each valley, with generally more incision upstream on the Varitis relative to the Kolokithas. Incision rates on the Varitis are roughly twice as high as on the Kolokithas, but the average incision rate of both valleys combined is comparable to coastal rock uplift rates derived from marine terraces. Collectively, our results suggest that fluvial systems are sensitive to climate and tectonic processes even when affected by geomorphic disturbances, like river capture and beheading. However, care must be taken when interpreting river terraces as direct records of climate and tectonic processes, particularly when working on a single river valley.

KEYWORDS
Crete, incision, Mediterranean, river capture, river terrace

1 | INTRODUCTION

River terraces are landforms that flank many fluvial valleys and are often used as archives of climate and tectonic processes (Bull, 1991; Lavé & Avouac, 2000; Pazzaglia and Brandon, 2001; Wegmann & Pazzaglia, 2002, 2009; Gallen et al., 2015; Pazzaglia, 2022; Marder, Gallen, & Pazzaglia, 2023). Conceptual models suggest that fluvial terrace formation results from changes in the sediment supply to water discharge ratio (Schumm, 1969). Periods with elevated sediment supply relative to water discharge allow for valley aggradation and lateral widening, whereas intervals of increased water discharge relative to sediment supply drive channel incision, floodplain abandonment and terrace formation (e.g. Bull, 1991; Pazzaglia, 2022). Changes in the sediment supply to water discharge ratio are primarily thought to be modulated by climate fluctuations, while the long-term incision rate reflects river response to rock uplift (Bull, 1991; Pazzaglia & Brandon, 2001). Within this conceptual framework, river capture events should also influence fluvial terrace formation by impacting sediment and water availability and transiently affecting river incision rates.

Several field-based studies have explored the impact of river capture (drainage area gain) or river beheading (drainage area loss) on river terraces (e.g. Stokes & Mather, 2000; Harvey et al., 2014; and references therein). Most of these studies focus on a captured or beheaded river, with some looking at river responses in both scenarios. These studies generally report how capture-induced changes in sediment flux and water supply influence river terrace formation, sedimentology and stratigraphy, and incision rates (García, 2006; García & Mahan, 2014; Maher, Harvey, & France, 2007; Mather, 2000; Stokes, Mather, & Harvey, 2002; Whitfield & Harvey, 2012). Changes in river terrace character (e.g. fill, strath, paired, unpaired) in response to capture vary among studies. However, most studies suggest that pre- and post-capture terrace emplacement is paced by Quaternary climate change, while evidence of river capture and beheading is archived in terrace stratigraphy and incision rates. To our knowledge, no study of the impact of capture has been performed on two adjacent rivers that share a common downstream confluence and, thus, local base level, and few studies have investigated how incision patterns change along captured and beheaded rivers.

In this study, we explore the impact of a geologically recent river capture on the formation and characteristics of Pleistocene and Holocene river terraces and incision rates and patterns with a detailed case study of the eastern portion of the Anapodaris River basin in south-central Crete, Greece (Figure 1). This represents one of the only studies of Pleistocene fluvial terraces from the island of Crete. The Anapodaris headwaters preserve geomorphic evidence of recent drainage area exchange between two adjacent tributary rivers, the Kolokithas and the Varitis. Both rivers are tethered to the same base level at their confluence, drain roughly the same amount of area, ~100 km^2 each, and their valleys are lined with river terraces that record the unsteady history of bedrock incision. This unique situation allows us to systematically study the impact of recent river capture on terrace formation and incision history along the main stem channels of the expanding (Varitis) and contracting (Kolokithas) drainages. To this end, we combine detailed mapping of river terraces, stratigraphic and soil development descriptions, topographic analysis, and luminescence geochronology to quantify river sedimentation (terraces) and incision history in response to capture and beheading. Our results provide general insight into river terrace formation but, more importantly, highlight the critical role of drainage area exchange in affecting the interpretation of climate and tectonic signals from river terraces.

2 | BACKGROUND

2.1 | Geology and geomorphology

Crete is a forearc high above the Hellenic Subduction Zone, where the African lithosphere subducts beneath Eurasia at a rate of ~35 mm/year, largely because of rollback of the African slab with smaller contributions from slow Africa–Eurasia convergence (Figure 1a) (Jolivet & Brun, 2010; Reilinger et al., 2006, 2010; Vernant, Reilinger, & McClusky, 2014). Crete exhibits pervasive upper crustal extension with both ~N–S and ~E–W striking active normal faults with slip rates between ~0.1 and 1 mm/year (Angelier et al., 1982; Caputo et al., 2010; Gallen et al., 2014; Nicol et al., 2020; Ott et al., 2019a; Peterek & Schwarze, 2004). Miocene to Pliocene marine sediments fill many of the grabens opened by extension. The surface exposures of these graben-filling sediments are currently up to hundreds of meters above sea level, documenting that long-term regional uplift outpaces the effects of upper crustal thinning (Meulenkamp, van der Zwaan, & van Wamel, 1994; van Hinsbergen & Meulenkamp, 2006; Zachariasse, van Hinsbergen, & Fortuin, 2008). Quaternary marine terraces along Cretan coastlines record rock uplift rates between ~0.1 and 0.3 mm/year in active normal fault hanging walls and as high as ~1 mm/year in normal fault footwalls (Gallen

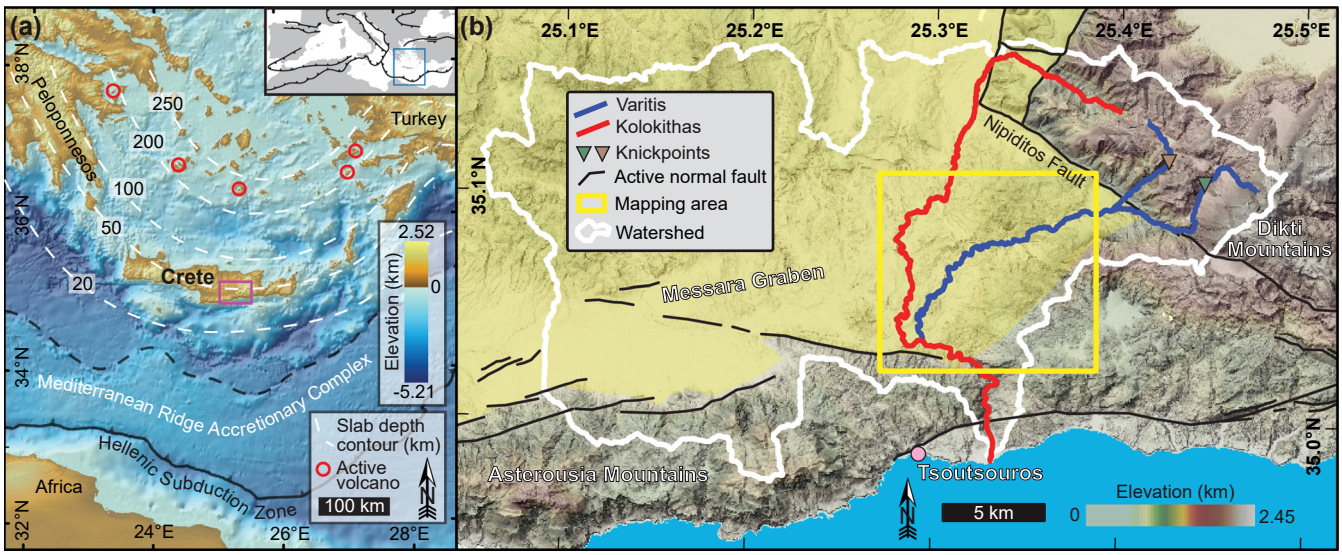

FIGURE 1 Tectonic setting and mapping area. (a) Generalised tectonic setting on a shaded relief map. Topography is from the ~90 m-resolution shuttle radar topography mission (SRTM) data, and the bathymetry is from the ~10 km-resolution GEBCO data. The purple box shows the map's location in Figure 1b. Inset shows the location of the main map in the blue box within the Mediterranean region with major active and inactive plate boundaries as black lines with teeth on the upper plate. (b) The Anapodaris watershed and the area mapped during this study. The area underlain by Neogene sedimentary basin fill is highlighted with yellow shading, approximating the extent of active extensional grabens. The yellow box shows the location of the mapping area, as shown in Figure 4a.

et al., 2014; Ott et al., 2019a; Robertson et al., 2019, 2023). High rock uplift rates are evident in deeply incised gorges and coastal rivers, and millennial-scale basin average erosion rates are between ~0.05 and 0.30 mm/year (Ott et al., 2019b). Upper crustal extension and high rock uplift rates on the island are thought to be driven by upper plate stretching because of retreat and gravitational instability of a crustal wedge thickened by rapid underplating (Angelier et al., 1982; Gallen et al., 2014; Ott et al., 2019a).

The Anapodaris drainage basin drains from the Dikti Mountains, a high-elevation carbonate massif, across the Messara Graben before flowing through a breached normal fault relay zone between the Asterousia and Dikti Mountains and discharging into the Mediterranean (Figure 1; Gallen et al., 2014; Gallen & Wegmann, 2017; Robertson et al., 2019). The Messara is an active graben filled with mostly Miocene to Pliocene marine sediments and lesser amounts of Quaternary fluvial sediments unconformably overlying these marine units. The rivers cutting across the basin are actively incising the basin fill, indicating a net erosional state.

2.2 | River terraces

River terraces provide a record of unsteady vertical stream incision and are commonly used to infer rates of base-level fall driven by processes including rock uplift. River terrace deposits are defined as allostratigraphic units with a lower unconformity, the 'strath,' and a flat upper surface referred to as the 'tread.' When thin (<3 m), river terraces are termed 'strath terraces' and are inferred to represent a past mobile alluvial layer overlying bedrock (Bucher, 1932; Bull, 1991; Wegmann & Pazzaglia, 2002). When valley aggradation pushes the river far above its strath, thick alluvial deposits are preserved and called 'fill terraces' (Bull, 1991). Importantly, river terraces, particularly strath terraces, represent the paleo-river bottom. Thus, differencing the elevation of a river strath from the modern channel bed represents the magnitude of the incision. Dating a terrace deposit approximates the time interval over which the incision occurred, allowing one to determine river incision rates.

Regardless of their classification, river terraces result from unsteady phases of vertical incision and lateral planation and widening associated with changes in the relative proportion of sediment supply and water discharge (Bull, 1991). While there is some ongoing debate (Bruni et al., 2021; Scherler et al., 2016), most studies infer that changes in sediment supply, *Qs*, and water discharge, *Qw*, are modulated by Quaternary climate change (Bull, 1991). In this conceptual framework, different climate states (warmer or cooler) or transitions between climate states perturb the system, driving changes in the *Qs*–*Qw* ratio and, thus, fluctuations between aggradation (and lateral widening) and vertical incision, resulting in the construction of river terraces (e.g. Pazzaglia, 2022). How climate variability during the Quaternary affects the *Qs*–*Qw* ratio, and phases of terrace development and bedrock incision vary from region to region. Several studies of Pleistocene deposits in Crete, which we discuss in more detail below in Section 2.4, suggest phases of aggradation during cooler (and wetter) periods (stadial and glacial), likely because of elevated *Qs*, with incision dominating during warmer (interstadial and interglacial) intervals because of a decrease in *Qs* and an increase in *Qw* (Nemec & Postma, 1993; Ott et al., 2023; Pope et al., 2008; Pope, Candy, & Skourtsos, 2016).

Given the connections between base-level fall rate and Quaternary climate, river terraces are often used as tectonic and climate archives. Under the assumption that the river profile remains relatively steady over geological time, river terraces serve as a proxy for rock uplift and crustal deformation (Lavé & Avouac, 2000, 2001; Pazzaglia & Brandon, 2001; Wegmann & Pazzaglia, 2009). When linked to climate, phases of terrace emplacement and periods of vertical river incision and terrace sedimentology can be used to understand the landscape and geomorphic response to climate change (Bull, 1991). However, additional geomorphic processes, such as meander bend cutoff (Finnegan & Dietrich, 2011; Limaye & Lamb, 2016; Pederson et al., 2024; Scheingross et al., 2020) and river capture (e.g. Stokes & Mather, 2000), can also affect vertical incision as well as *Qs* and *Qw* but are less well studied in natural systems.

2.3 | Previous studies of the impact of river capture on terraces

Several case studies have explored the role of river capture and beheading on river terrace formation and incision rates (Stokes & Mather, 2000; Mather, 2000). Stokes, Mather, and Harvey (2002) studied the impact of river capture and beheading on river systems in the Sorbas Basin in southeastern Spain. These authors focused on changes in incision rate, sediment flux, and base level lowering using terraces on rivers variably affected by drainage reorganisation. They document increases in incision rate and sediment flux in the capturing drainage (area gain) and a reduction of incision rates on the beheaded river (area loss).

Maher, Harvey, and France (2007) and Whitfield and Harvey (2012) studied the fluvial system and river terrace response along the Rio Alias in southeastern Spain in response to a drainage area loss of ~70% at 70 ka. They document changes in bedform geometry in terrace sediments, including decreases in bedform height, channelisation, and maximum clast size in terraces younger than the beheading. They infer significant reductions in water and sediment supply following the beheading and a decline in incision rate post-capture relative to adjacent rivers. Quaternary climate change was inferred to pace phases of channel aggradation and vertical incision pre- and post-capture.

García (2006) and García and Mahan (2014) studied river terrace morphology and emplacement timing along San Lorenzo and Pancho Rico Creeks that drain across the San Andreas Fault in Gabilan Mesa, CA. Pancho Rico Creek captured the headwaters of San Lorenzo Creek, producing a distinct change in terrace morphology on Pancho Rico Creek. San Lorenzo maintains thick fill terraces that predate the capture. In contrast, Pancho Rico Creek's pre-capture terraces are classic, well-developed paired strath terraces, and post-capture are thinner and unpaired. This change in terrace character is attributed to shifts in sediment and water supply afforded by the increase in drainage area coupled with access to more indurated lithologies within the captured area. Studying channel reversal along escarpment divides in the Negev Desert, Israel. Harel et al. (2019) showed that river terraces on captured upland rivers can preserve paleo-river gradients before the drainage capture (reversal) occurred.

These studies highlight changes in terrace deposition and morphology, clast provenance, sediment and water flux, and incision rate

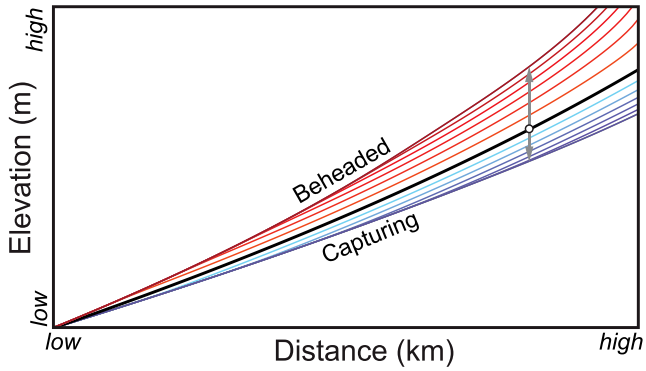

FIGURE 2 Conceptual model for an equilibrium river profile (back line) perturbed by capture (blue lines) or beheading (red lines). Each line below the original equilibrium river profile represents an equal time step in the evolution of the longitudinal profile towards new area-adjusted gradients.

in response to capture. They demonstrate that rivers subjected to a drainage area gain or loss will experience an increase or decrease in incision rate, respectively, and thus modification of the longitudinal profile. This effect occurs because if we assume the river profile is graded and adjusted to the base level fall rate before changes in drainage area, after reorganisation, the local river gradient is out of equilibrium, driving river profile adjustments through changes in the incision or aggradation rate. The effect of drainage reorganisation on a river's longitudinal profile is conceptually shown in Figure 2. Following the perturbation caused by drainage reorganisation, the longitudinal profile of a stream that gains area (capturing) will evolve towards a gentler slope (Figure 2). In contrast, a stream that loses area (beheaded) will trend towards a steeper longitudinal profile gradient (Figure 2). While the insights gained are significant, further studies can help identify emergent generalities that can help isolate the relative roles of exogenic and autogenic processes in terrace formation and bedrock river incision patterns.

2.4 | Quaternary climate and geomorphology on Crete

Quaternary climate change is thought to strongly influence weathering, sediment production, transport and deposition, and runoff that drives unsteadiness in hillslope sediment supply, water discharge, and pace river aggradation and incision (Bull, 1991). This view largely stems from work in temperate climates, and studies in the Mediterranean suggest that the geomorphology of this region is particularly sensitive to Quaternary climate change (e.g. Coltorti & Dramis, 1995; Macklin et al., 2002; Rose, Meng, & Watson, 1999; Wegmann & Gallen, 2022; Wegmann & Pazzaglia, 2009). Several studies conducted on Crete document strong links between Quaternary climate change and phases of aggradation and incision, largely focused on alluvial fans (Nemec & Postma, 1993; Ott et al., 2023; Pope et al., 2008; Pope, Candy, & Skourtsos, 2016). These studies consistently show that phases of fan aggradation are associated with cooler intervals (stadials), and periods of incision occur during warmer climate conditions (Nemec & Postma, 1993; Ott et al., 2023; Pope et al., 2008; Pope, Candy, & Skourtsos, 2016). These results are consistent with data from elsewhere in Crete that show periods of alluvial fan aggradation are typical during cooler climate intervals (Gallen et al., 2014; Wegmann, 2008), and incision occurs during relatively warmer interstadials (Pope et al., 2008; Pope, Candy, & Skourtsos, 2016).

Ott et al. (2023) used modern and paleo-denudation rate measurements from cosmogenic nuclides to further demonstrate that during climate oscillations, basin average denudation rates do not change significantly during these phases of aggradation and incision. From these data, they infer that Quaternary climate changes do not considerably affect denudation but rather pace sediment transport. Ott et al. (2023) suggest that climate-controlled variations in runoff and hillslope vegetation primarily drive changes in sediment transport. During cooler, drier glacial and stadial intervals, reduced hillslope vegetation releases sediment to channels, which aggrade because of limited runoff. During warmer, wetter interglacials and interstadials, increased hillslope vegetation stabilises sediment supply, and increased runoff enables incision to commence. These results are consistent with the conceptual models Bull (1991) envisioned for climate-driven terrace genesis.

3 | METHODS

3.1 | Digital topographic analysis

We used a 5-m digital terrain model (DTM) provided by the Hellenic Cadastre SA to conduct river profile analysis and project river terraces onto valley profiles using TopoToolbox v2 (Schwanghart & Scherler, 2014) and ChiProfiler (Gallen & Wegmann, 2017) Matlab functions. We conducted standard surface hydrology modelling by filling sinks and determining flow directions and accumulation. Using these products, we defined the stream network as areas draining ≥1 km^2, a commonly used value to define the start of the fluvial network. We extracted the main stems of the Kolokithas and Varitis Rivers and plotted longitudinal river profiles.

We calculated the transformed distance coordinate, χ, for each of the main stem rivers:

$$\chi = \int_{x_b}^{x_c} A(x')^{-\theta_{\text{ref}}} dx' \quad (1)$$

where x is the streamwise distance; x_b and x_c are the distance at an arbitrary base level and distance at the channel head, respectively; A is the drainage area, and θ_{ref} is the reference concavity index (Perron & Royden, 2013). We used the most common value found in the literature for the concavity index of 0.45 to make results comparable with other studies.

Plots of χ versus elevation, called χ-plots, are useful because they act to remove concavity of the river profile geometry, linearising it such that the slope of the plot is the normalised steepness index, k_{sn}. This is most easily seen with Flint's (1974) law that describes the relationship between local channel slope, S, and drainage area, A, as a power function:

$$S = \frac{dz}{dx} = k_{sn} A(x)^{-\theta_{ref}} \quad (2)$$

Integrating Flint's law for distance, x, predicts the elevation of the river network from a given base-level position, x_b:

$$z(x) = z(x_b) + k_{sn}\chi \quad (3)$$

Equation 3 has the form of a line, such that the slope of the χ-plot is the normalised steepness index, k_{sn} (Gallen, 2018; Gallen & Thigpen, 2018).

χ and χ-plots help determine the channel steepness and can be used to test for geologically recent river capture. River capture and beheading will distort χ-plots, and if corrected to the pre-capture drainage area, both rivers will collapse on the same χ-elevation trend (Giachetta & Willett, 2018; Willett et al., 2014). Put another way, this analysis can help evaluate the fidelity of inferred captures. From inspection of the DTM, we inferred the point of river capture between the Varitis and Kolokithas Rivers in the Dikti Mountains based on the presence of knickpoints. We used these locations to guide an experiment, where we digitally removed the drainage area above the knickpoints from the Varitis River, added the same area amount to the Kolokithas, and recalculated χ to test for evidence of river capture.

We project mapped terrace polygon outer edges (mapping details provided in the following section), assumed to approximate strath elevations, onto centre lines that trace the Varitis and Kolokithas River valleys (cf. Marder, Gallen, & Pazzaglia, 2023). We fit smoothed lines through the projected terrace elevations using the constrained regularised smoothing (CRS) algorithm in TopoToolbox with a 10^5 smoothing factor (Schwanghart & Scherler, 2017). Terrace outer edges and smoothed fit elevations were plotted as a function of distance along the valley centre lines, and the modern river elevations were plotted for reference. To visualise incision patterns, we subtract the local elevation of the terrace from the modern channel and plot results as a function of distance along the valley.

3.2 | Mapping

We mapped river terraces along the Kolokithas and Varitis Rivers at the 1:10,000 scale. We used a combination of digital topographic maps and satellite imagery to map precise terrace locations, taking care to map the basal unconformity (i.e. strath) of alluvial deposits with the underlying bedrock. Kinematic GPS (KGPS) and a laser range finder were also used to determine the precise elevation of strath contacts both with respect to the geoid and relative to the modern channel elevation while in the field. Terraces were correlated in the field based on soil profile development as determined by detailed descriptions of exposed soil profiles, colour of B_t soil horizons, stratigraphic and sedimentary characteristics, and loosely based on elevation above the modern channel. Soil colour was determined to be the best indicator of relative terrace age. We also used similar methods to map and describe other Quaternary deposits in the study area, most commonly alluvial fans.

Field maps were digitised using a 5-m DTM in ArcGIS Pro 2.4.0. We used a composite of elevation and slopeshade to refine the field maps based on the high-resolution DTM. Slopeshade maps overlay a standard hillshade and slope map, enabling better illumination and definition of terrace risers and allowing us to map terrace contacts more precisely. The field maps, elevation and slopeshade products, and field KGPS and laser range finder results were used to delineate straths as the river-facing traces of individual terrace polygons. We initially classified terraces by relative ages as mapped in the field and iteratively updated the classifications based on elevation patterns of terrace valley profiles. To check for misidentification of terrace units, we drew lines that followed the two main river valleys and projected the elevations of terrace units flanking each river on the valley lines. Terrace elevation plotted as a function of distance along the line aids in identifying potentially misclassified terraces as those displaying abrupt (step-function-like) changes. While most of the initial terrace unit assignments produced smooth valley profiles, in a few locations, field-mapped terraces were miscorrelated. We then adjusted the terrace unit assignment and iterated on this process until all obvious misclassifications were remedied before finalising our map.

3.3 | Geochronology

Fine-grained layers or lenses of quartz-rich sediment from fluvial terraces or overlying (i.e. capping) loess deposits were collected for optically stimulated luminescence (OSL) burial dating. We collected samples by hammering a ~25 cm light-proof metal cylinder into the target layers. After sample extraction, we collected moisture samples from the sample region, sealed them in airtight film containers and taped them closed. Finally, we collected samples for environmental dose rate (radiation) measurements within ~25 cm^3 around the luminescence sample.

Samples were analysed at Laber Scientific Luminescence Dating Laboratory using standard laboratory preparation techniques, including sieving, gravity separation and acid treatments in hydrochloric acid (HCl) and hydrofluoric acid (HF) in a darkroom to obtain the quartz fraction of analysis. The single-aliquot regenerative dose (SAR) technique was used for equivalent dose (De) measurements on 24 aliquots for each sample (Rhodes, 2011). The reported De represents an all-aliquot average and associated standard error for each sample. Depth, altitude and geomagnetic latitude determined the cosmogenic dose rate. The U, Th and K concentrations were measured from the sample using neutron activation analysis and converted to annual dose rate after considering the effect of water content.

4 | RESULTS

4.1 | Topographic analysis

Despite comparable drainage area and underlying bedrock, river profiles and χ-plots show that the Varitis is nearly twice as steep as the Kolokithas River; in the mapping area, the normalised steepness index of the Varitis is ~170 $m^{0.9}$, whereas the Kolokithas is ~90 $m^{0.9}$ (Figure 3). The χ profiles of both rivers are distorted in a way consistent with river capture (Figure 3). The capturing Varitis river is shifted to the left in the χ-plot and contains large knickpoints, while the Kolokithas is distorted down and to the right and does not contain

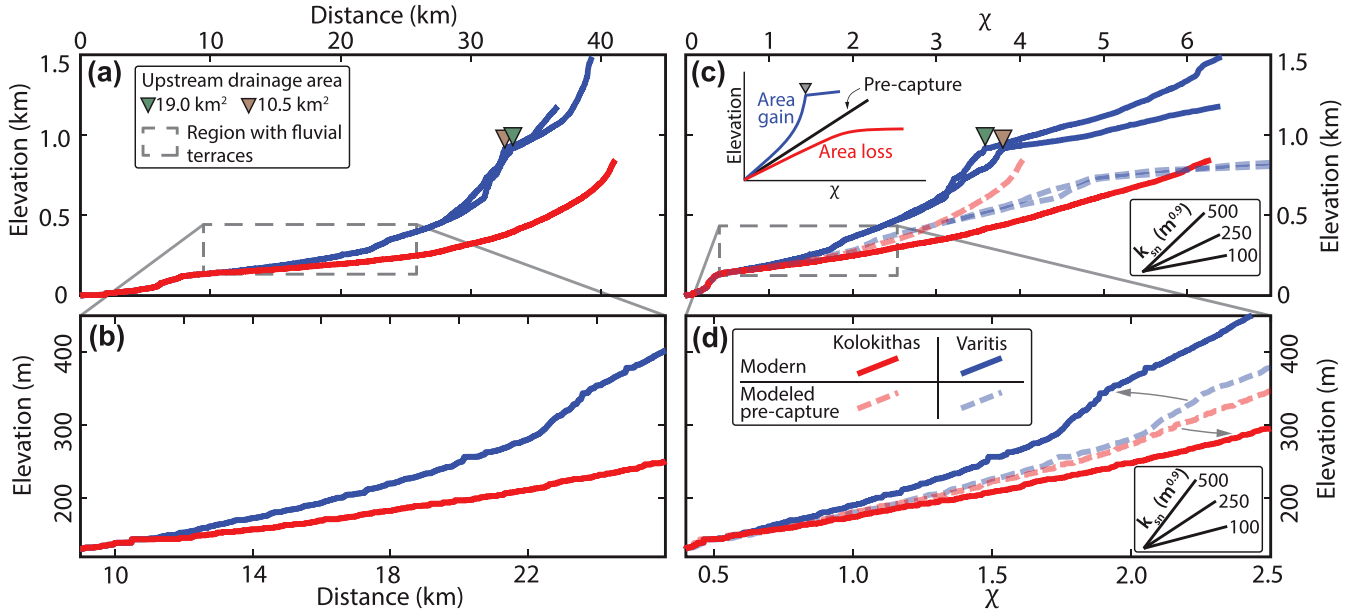

FIGURE 3 River profiles and analysis. (a) Kolokithas (red) and Varitis (blue) river profiles with major knickpoints (triangles) (location shown in Figure 1b). (b) River profiles as in Figure 3a but zoomed into the region with river terraces. (c) Derived χ-plots of the Kolokithas (solid red line) and Varitis (solid blue lines) with major knickpoints (triangles). The dashed red and blue lines show the modelled χ-plots for the Kolokithas and Varitis Rivers, respectively, after removing ~30 km^2 of drainage area (drainage area above the knickpoints) from the Varitis and adding it to the Kolokithas before calculating χ. The inset plot shows hypothetical χ-plots for a pre-capture river (black line) that either gains (blue line) or loses (red line) upstream drainage area through a capture event. (d) It is the same as in Figure 3c but zoomed into the approximate region with river terraces. Note that the χ-plots collapse in the area with terraces when χ is calculated with the modelled change in the drainage area.

knickpoints (Figures 1b and 3). Selecting the positions of major knickpoints on the Varitis as capture points, we estimate the Varitis captured ~30 km^2 of drainage area from the Kolokithas (Figures 1b and 3). Because there are two knickpoints, there were likely two capture events, one each on the western and eastern headwater branches of the Varitis (Figures 1b and 3c,d). Removing the combined area of capture from the Varitis, adding it to the Kolokithas, and then recalculating χ, the χ profiles collapse on top of one another and have nearly identical steepness, ~120 $m^{0.9}$ (Figure 3c,d). This analysis suggests that the two rivers were near a steady state with the base-level fall rate before the drainage area exchange.

4.2 | Quaternary deposits

4.2.1 | River terraces

We identified five unique river terrace levels along the Varitis River valley and four along the Kolokithas Valley (Figure 4). All river terraces are defined by a basal conglomerate with thicknesses varying from ~0.25 to 8 m (Figure 5). Most terrace conglomerates are capped by a package of finer-grained sediments, mostly sands, silts and muds of variable thicknesses, depending on the terrace level (Figure 5). In some cases, the fines represent overbank facies, and in other cases, younger capping loess. Terrace soils, particularly B_t horizons, mature, brown and redden with increasing elevation from the river channel (see Supporting Information for detailed soil profile descriptions of Pleistocene terraces). Based on relative elevation above the river channel, soil development, and stratigraphic and sedimentological characteristics, we assign terraces to five relative age classifications: Q_{t5} (youngest) to Q_{t1} (oldest), described in the succeeding texts.

Q_{t5} is characterised by a ~0.25–0.5 m thick pebble-to-cobble basal conglomerate capped with ~0.5–1.5 m of silty overbank facies sediment on the Varitis and ~1–3 m on the Kolokithas (Figures 5 and 6). Soil development is minimal, with minor clay and carbonate accumulation in a nascent B_t horizon. The strath is commonly observed between 0.25 and 3 m above the local channel level on both rivers, with strath exposures higher and more common on the Varitis than the Kolokithas (Figure 6). In some locations, Q_{t5} appears to be indistinguishable from the modern flood plain. We assign the lowest terrace on the Kolokithas to Q_{t5} because it grades to the same elevation as Q_{t5} at the confluence with the Varitis River. However, unlike the Varitis, the Kolokithas does not have a Q_{t4} terrace, so Q_{t5} on the Kolokithas likely formed over the same time interval as Q_{t4} and Q_{t5} on the Varitis.

Q_{t4} is only observed on the Varitis and is easily identified as having a thin (~0.25–0.5 m) basal conglomerate topped with a 2–3 m sequence of fine sediments (Figure 5). The fine sediments are largely overbank facies and show some stratification with course sand horizons present. Pottery shards of unknown age are scattered throughout the fine-grained overbank sediments. Soil development is weak and slightly more mature than Q_{t5}, with a thicker A horizon and a slightly more clay-rich and browner B_t horizon. Strath exposures are common with elevations ~3–8 m above the local channel (Figure 6).

Q_{t3} is well-preserved in both rivers and consists of a 1.0–2.5-m thick basal conglomerate capped with ~1.0–1.5 m of finer silts and sands (Figure 5). The lower portion of the finer layers have sand lenses, which leads to the interpretation that they represent overbank facies (Figure 5). Higher in the section, only silt is observed and interpreted as loess. The soil developed in the terrace deposits is relatively mature, with a well-developed, brown, clay-rich B_t horizon. The tread is typically laterally extensive and used for olive farming. The strath is

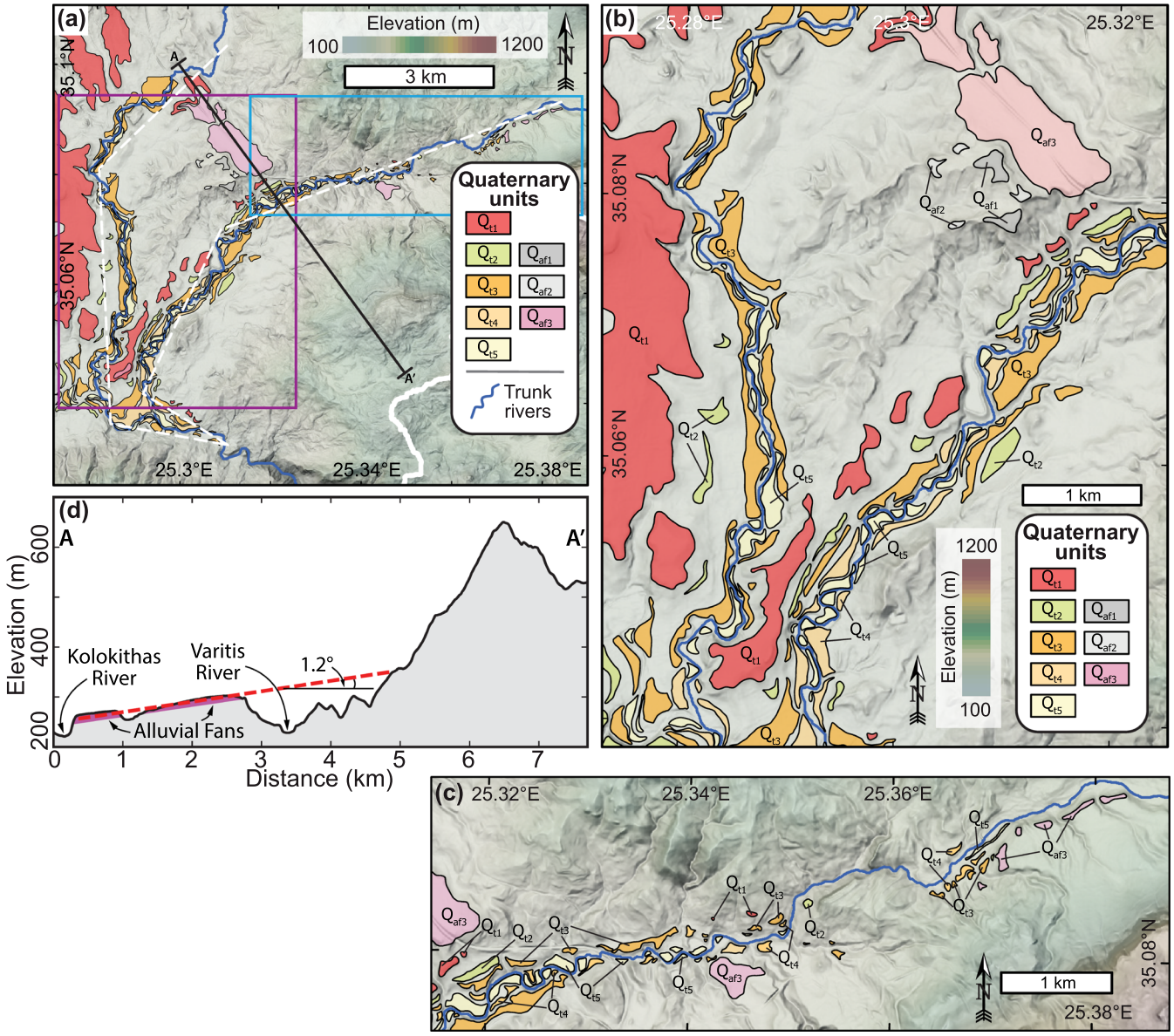

FIGURE 4 Mapped Quaternary deposits along the Kolokithas and Varitis river valleys. (a) Distribution of Quaternary units mapped in the study area classified by relative age and deposit type. The purple box shows the extent in Figure 4b, and the cyan box shows the extent in Figure 4c. The black A to A′ line shows the location of the annotated topographic profile in Figure 4d. The dashed white lines show the trace of the valley profiles to which terrace elevations are projected in Figure 7. (b) Enlarged map of Quaternary deposits along the Kolokithas and Varitis River valleys. (c) Enlarged map of the Quaternary depositions along the upper portion of the Varitis River valley. (d) The topographic profile in Figure 4a shows the constructional surface slope of the Q_{af1} alluvial fan between the Kolokithas and Varitis River valleys. The dashed red line is a linear regression using the surface elevation of the alluvial fan extent projected to the foot of the Dikti Mountains.

well-exposed on the Varitis and ranges between ~10 and 18 m above the local channel elevation (Figure 6). On the Kolokithas, the strath is not well exposed because the aggradation of the inset Q_{t5} terrace obscures it. Based on the few exposures and approximations based on observed thicknesses of Q_{t5} and Q_{t3}, the Q_{t3} strath on the Kolokithas is between ~5 and 13 m above the local channel elevation (Figure 6).

Q_{t2} is poorly preserved on both rivers, but patches are observed throughout the mapping area (Figure 4). The sedimentology and stratigraphy are more complex than the lower deposits, consisting of ~1.5 to 2.0 m of cobbles and course sands before transitioning to silty-to-sandy 0.4-m thick overbank facies capped by several decimeters of loess (Figure 5). The soil is well-developed, with high clay concentration in the B_t horizon and a distinct reddish-orange colour (Figure 5). The Q_{t2} strath is ~20–25 m above the Varitis River and ~18 m above the Kolokithas River (Figure 6).

Q_{t1} is an extensive deposit that flanks and locally forms the interfluve between both rivers near their confluence (Figure 4). The deposit is distinct on each river. On the Varitis, Q_{t1} is a typical strath terrace with ~1.5 m of conglomerates capped by ~0.5 m of finer-grained overbank material (Figure 5). On the Kolokithas, Q_{t1} is a thick fill terrace of ~7.5 m cobbly conglomerates capped by 0.5–1.0 m of finer sands (Figure 5). The soil on this deposit is distinctly well-developed, with a red B_t horizon that can be seen clearly on satellite images. Its tread is extensive and is commonly used for olive farming. The strath is well exposed on both rivers and ranges from ~25 m near the confluence to nearly 40 m above river level farther upstream (Figure 6).

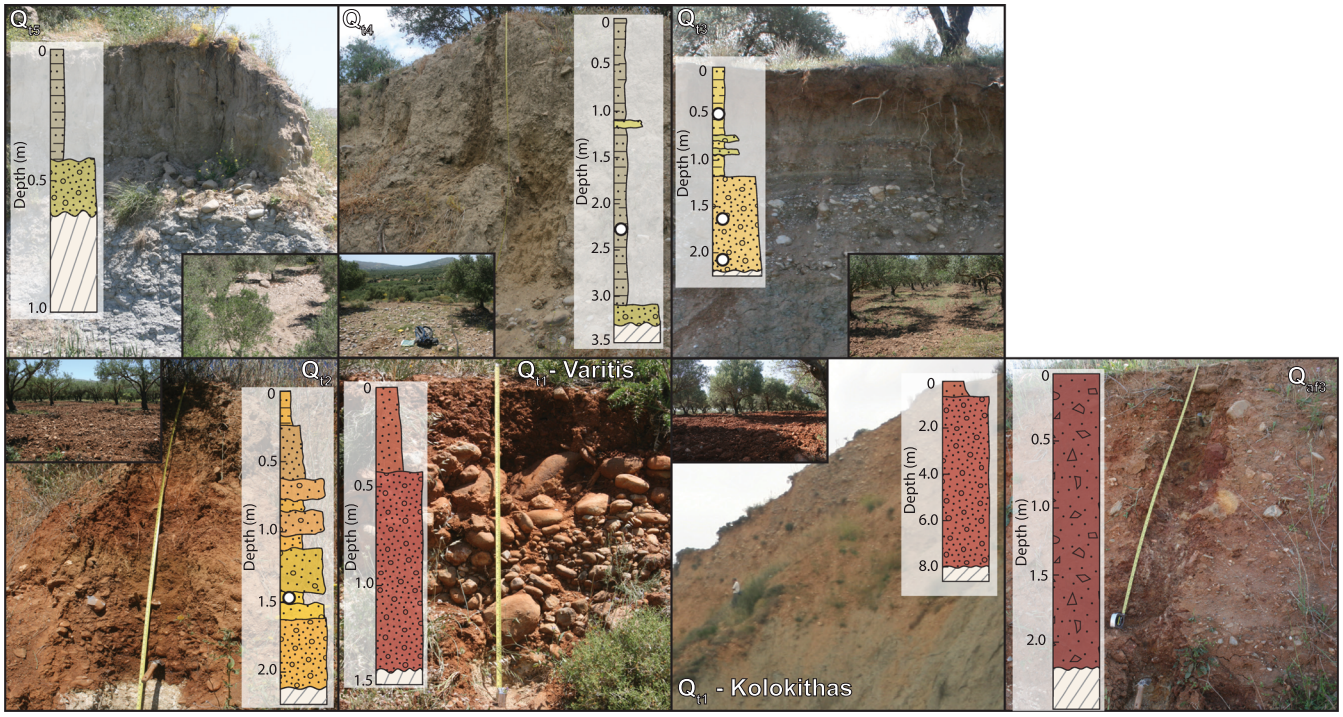

FIGURE 5 Quaternary unit photos and stratigraphic columns. Panels show river terraces from youngest to oldest (reading rows from left to right) as captured in photos and stratigraphic descriptions. The white dots in some stratigraphic columns show the location of luminescence samples collected within the stratigraphy. Note that in Q_{t3}, samples were not collected in the same location. The inset photos show the surface colour of the soil. Also shown in the lower right is Q_{af1}. The description is from the highest part of the fan adjacent to the Varitis. The fan deposits are thinnest here, thickening several meters toward the northwest.

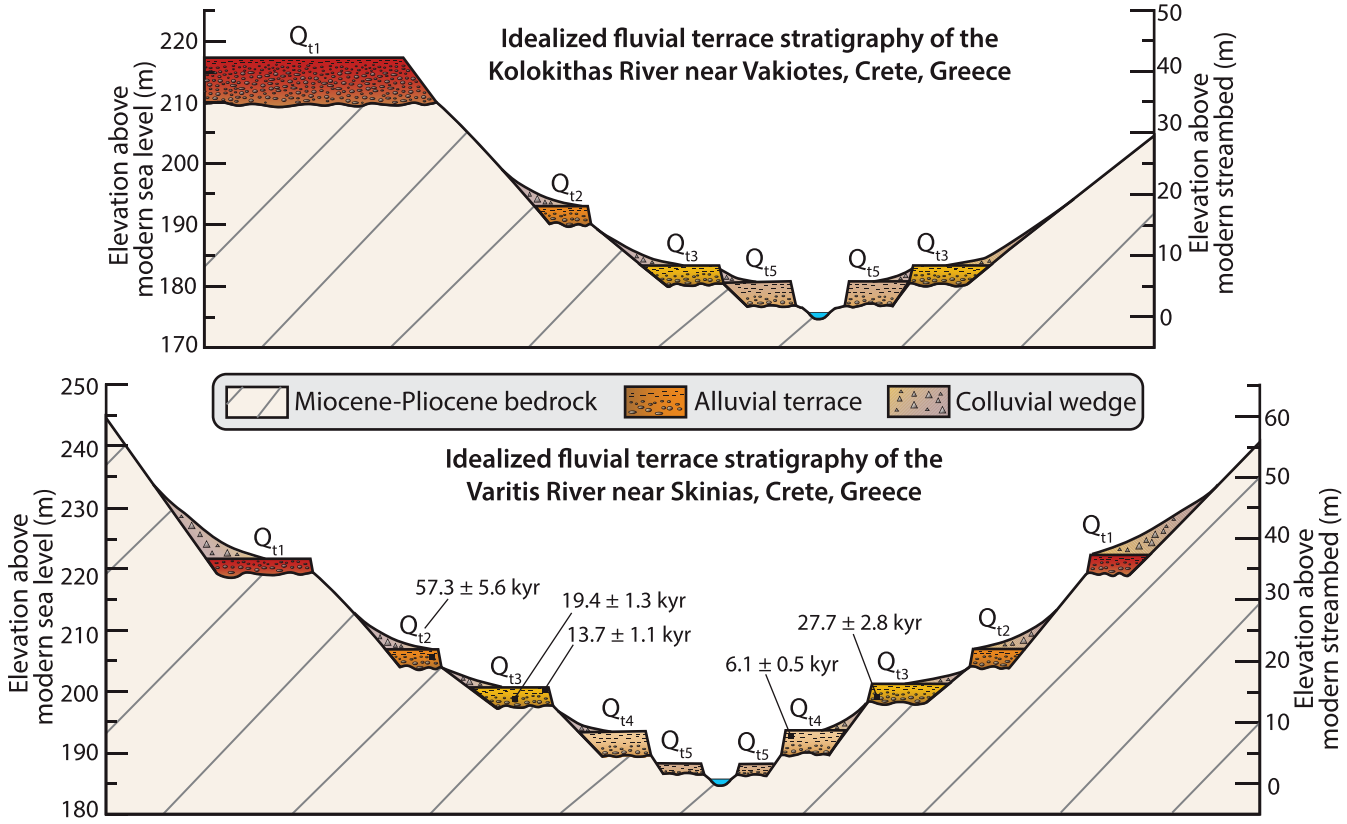

FIGURE 6 Graphical representation of terrace stratigraphy in representative locations. The top panel shows an idealised terrace stratigraphy for the Kolokithas River. The bottom panel shows an idealised terrace stratigraphy for the Varitis River, along with the approximate stratigraphic position and age of optically simulated luminescence samples. Note that the observed terrace elevations change with streamwise distance along both rivers, and samples obtained are not necessarily from this location. The vertical scales on both plots are the same.

4.2.2 | Alluvial fans

We find evidence of three distinct phases of alluvial fan sedimentation in the mapping area. Most of the alluvial fans are located in the upper portions of the Varitis River, where the carbonate massifs shed sediment into the adjunct Messara graben (Figure 4). These deposits are easily observed in map view topography and satellite imagery, and sedimentologically, they are more poorly sorted with more angular clasts relative to the river terraces (Figure 5). Soil development in fan exposures is comparable but slightly more mature than Q_{t1} (Figure 5). We assign these terraces to the youngest relative age group for alluvial fans, Q_{af3}.

An alluvial fan complex was identified between the Varitis and Kolokithas Rivers (Figure 4). Mapping and the degree of soil development suggest at least three different phases of fan deposition. Q_{af3} is an extensive deposit that shares sedimentological and soil characteristics with the smaller fans in the Varitis headwaters, so we assign it to the same unit, Q_{af3}. The fan surface slopes ~1.0°–1.5° to the NW, and a road cut exposes the basal unconformity, which maintains a similar NW slope (Figure 4). The fan surface slope indicates a source from the SE in the Dikti Mountains, but this fan complex is currently disconnected from the Dikti Mountains because of the incision of the Varitis River valley below the fan's aggradational surface (Figure 4). Q_{af2} and Q_{af1} are highly eroded and patchy (Figure 4). Soils developed on these fans are calcretes (B_k horizon) with clasts cemented in a pedogenic carbonate matrix, indicating a mature age. Q_{af2} is nearly identical to Q_{af1}, but based on mapping, it is inset and, therefore, a younger unit (Figure 4).

4.3 | Geochronology

We report five new OSL ages from three terraces: Q_{t4}, Q_{t3} and Q_{t2} (Figures 5 and 6). We sampled Q_{t4} in the middle of the ~3 m thick package of fine sediments and obtained a depositional age of 6.1 ± 0.5 kyr. This age is in line with observed pottery shards in this deposit, and it also constrains the age of Q_{t5} to the Holocene. We collected three samples from Q_{t3}. We sampled from sandy lenses within the conglomerate units in two locations and collected one sample from the overlying loess (Figure 5). The two samples within the conglomerate yielded ages of 27.7 ± 2.8 and 19.4 ± 1.3 kyr. The loess cap produced an age of 13.7 ± 1.1 kyr. The one sample collected from Q_{t2} was from a sand lense ~1 m above the strath and gave a depositional age of 57.3 ± 5.6 kyr. The OSL results are all in stratigraphic order with older ages in successively higher terraces. Within Q_{t3}, where we have multiple samples, the OSL ages young moving up section.

4.4 | River incision patterns

The steepness of river terraces and incision patterns along each valley differ (Figure 7). Consistent with the differences in river profile steepness (Figure 3), the terraces on the Varitis have a steeper gradient than those on the Kolokithas (Figure 7a,b). The patterns of incision change with terrace level on the Kolokithas. Q_{t1} has the most incision upstream and the least downstream, but Q_{t2} and Q_{t3} show the most incision downstream and the least upstream (Figure 7c). Q_{t5}

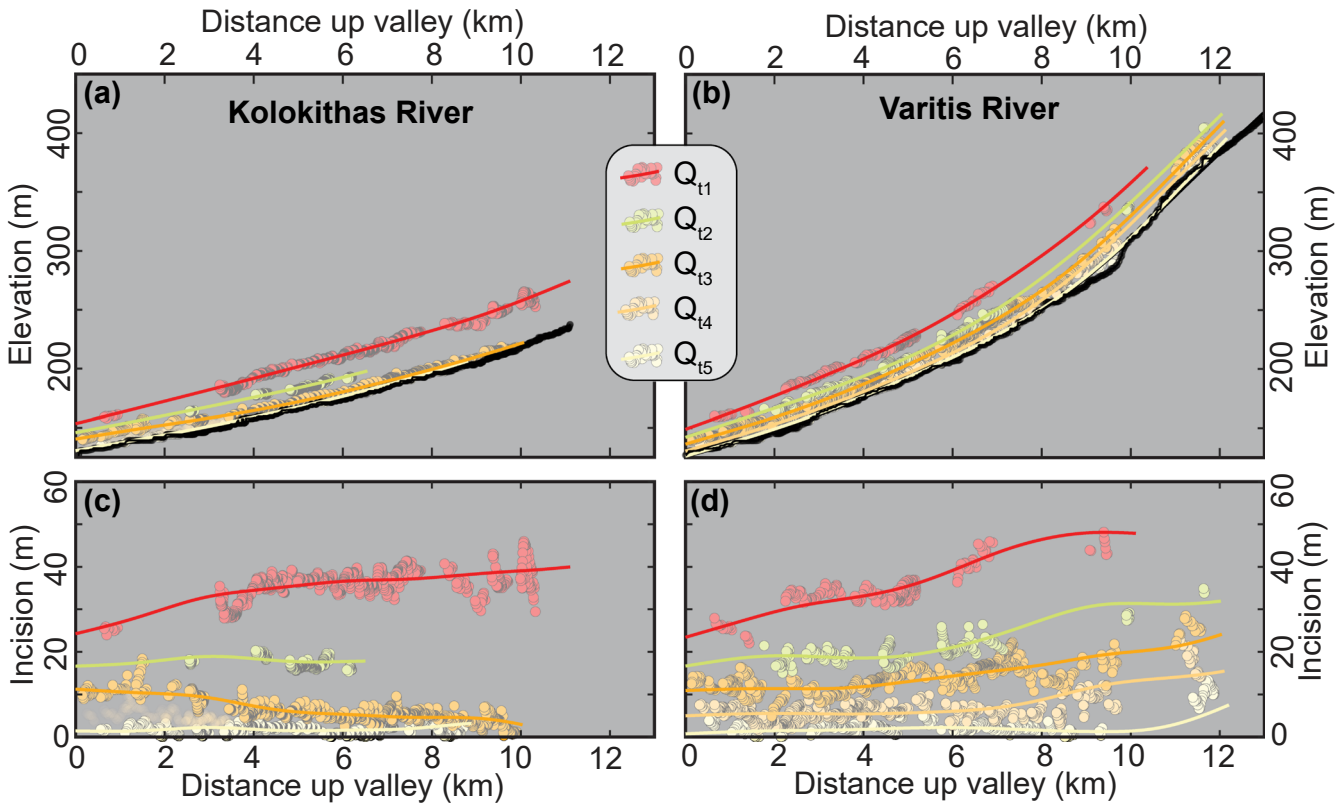

FIGURE 7 Down valley profiles showing terrace elevations and incision patterns projected onto the dashed white valley profile lines shown in Figure 4a. (a) Along valley terrace and river elevations (black line) along the Kolokithas River. (b) Same as in Figure 7a but for the Varitis River. (c) Incision patterns along the Kolokithas River valley; note the transparent points in the background are associated with Q_{t4} on the Varitis. (d) Same as in Figure 7c but for the Varitis River. Note the steeper river and terrace profile gradient of the Varitis relative to the Kolokithas on the top row. On the bottom row, note the difference in incision patterns between the two rivers.

shows relatively consistent incision patterns along the Kolokithas Valley (Figure 7c). In contrast, on the Varitis, the incision magnitude increases moving upstream for all terraces, with the older terraces showing the largest difference in downstream to upstream incision magnitudes (Figure 7d).

5 | DISCUSSION

5.1 | Topographic evidence of river capture

River profile analysis demonstrates a topographic signature of river capture and beheading on the Varitis and Kolokithas Rivers, respectively (Figure 3c, d). Both rivers have comparable modern drainage areas; the Varitis is ~93 $km^{2,}$ and the Kolokithas is ~105 km^2 (Figure 3). Yet the normalised steepness index of the Varitis is nearly double that of the Kolokithas within the Messara graben despite cutting through comparable rock types (Figure 5d). The difference in steepness for comparably sized rivers suggests disequilibrium gradients. This interpretation is supported by the χ analysis that shows the distortion of the modern χ profiles consistent with the Varitis River capturing the Kolokithas' headwaters (Figure 3c, d). Based on the inferred capture locations provided by the western and eastern tributary knickpoints in the Varitis (Figures 1 and 3), ~30 km^2 was captured by the Varitis, and our pre-capture χ-profile reconstructions that indicate the river profiles have nearly identical steepness within the Messara graben (Figure 3c,d). Given that there are two knickpoints in the Varitis, one each on the west and east headwater tributaries (Figure 1b), two captures likely took place; however, we do not know the relative timing of these events. Downstream geomorphic constraints allow us to place estimates on the timing of the initial capture, and we later speculate on the relative timing of both captures based on these results and changes in incision rate along the Varitis River.

The precise mechanism that drove capture is unknown, but we assume it relates to changes in slip rate along the Nipiditos Fault. The paleo-coarse of the Kolokithas River in the Nipiditos footwall appears structurally controlled as it follows a linear path parallel to the strike of the Nipiditos Fault (Figure 1b). Unlike several more N–S striking faults in the area, the WNW–ESE striking Nipiditos Fault, while assumed to be active during the Quaternary, does not have evidence of Holocene ruptures (Nicol et al., 2020). Given the prominent topographic expression of this fault, it was likely more active in the past and more recently activity waned. If correct, the slowdown in fault slip rate would cause rivers draining the footwall over the fault (i.e. the Varitis River) to relax gradient and lengthen in the headward direction, possibly driving capture.

5.2 | Interpretation of terrace ages

Our geochronology is consistent with previous studies in Crete that suggest Pleistocene river valley aggradation phases occur primarily during cooler periods (Figure 8; Pope et al., 2008; Pope, Candy, & Skourtsos, 2016; Ott et al., 2023). Our results indicate that the Q_{t3} deposit aggraded over a nearly 10 kyr period associated with the last glacial maximum (marine isotope stage [MIS] 2), and Q_{t2} was deposited during MIS 4. Based on these results and the previous studies that link cooler periods to fluvial aggradation, we infer that Q_{t1} was deposited during MIS 6. The degree of soil development on Q_{t1} is slightly more mature but comparable to alluvial fans dated to ~100 kyr ~ 75 km west at the Preveli Gorge (Runnels et al., 2014) and a marine terrace dated to ~125 kyr ~ 8 km south near the coastal town of Tsoutsouros (Figure 1b; Gallen et al., 2014), supporting this interpretation.

The Holocene aggradation and incision phases are inferred to represent anthropogenic perturbations rather than climate change, although we cannot rule out the latter. This interpretation largely stems from the differences in stratigraphy and sedimentology of the Holocene terraces compared to the Pleistocene terraces. The Holocene terraces have thin cobbly lags (≤50 cm) topped with a thick (0.5–3.0 m) accumulation of fines. Most Pleistocene terrace exposures have thicker cobbly lags (≥1.0 m) with typically thinner finer-grained caps (≤0.5 m), although fines on the Pleistocene terraces can locally be thicker when proximal to hillslopes. We attribute the thick accumulation of fines on the Holocene terraces as a result of anthropogenically induced soil losses because of deforestation, agricultural and other land use changes that likely pace hillslope sediment supply and thus phases of valley aggradation (Rackham & Moody, 1997). Since the mid-Holocene, Dusar et al. (2011) proposed a regional synthesis for Eastern Mediterranean fluvial basins, demonstrating that the timing and drivers of Holocene sediment dynamics, allowing for temporal variability at the local scale, can be explained by human-landscape impacts through forest clearing and burning for agriculture and pastoralism and the subsequent rapid increase in regional rates of soil erosion. Importantly, a comparison of flood frequencies from Holocene lacustrine and fluvial records from Crete (Benito et al., 2015; Jouffroy-Bapicot et al., 2021; Macklin et al., 2010) or from the Eastern Mediterranean region (Benito et al., 2015; Dusar et al., 2011) does not show any clear regional pattern that could argue for climate as a dominant driver of Holocene flood history, and thus fluvial aggradation associated with the Q_{t4} or Q_{t5} terraces.

We do not have absolute age control on the alluvial fans in the study area. However, based on the degree of soil development and clast weathering (Figure 5), we infer that Q_{af3} is somewhat older than Q_{t1}. Given the degree of soil development, the elevation of the Q_{af3} between the Varitis and Kolokithas Rivers, and the observation that Q_{t1} incises Q_{af3} in the Kolokithas, we assign Q_{af3} deposition to MIS 8. As such, Q_{af2} and Q_{af1} are older and perhaps related to aggradation during MIS 10 or MIS 12. Importantly, the Q_{af3} fan deposit between the Varitis and Kolokithas Rivers must have been deposited before the Varitis captured the Kolokithas headwaters. This follows because, based on the fan slope, it was shed from the Dikti Mountains to the SE (Figure 4c), and it is currently cut off from this sediment source because of incision along the Varitis. These observations and age inferences suggest that the capture occurred between MIS 8 and MIS 6, ~150–250 kyr.

5.3 | Terrace genesis and incision history

Important differences exist in terrace stratigraphy, incision patterns and incision rates between the valleys. On the Varitis, there are five vertically separated strath terraces so that straths are above treads of successively lower (younger) units (Figure 6). In contrast, there are four terrace levels on the Kolokithas, with less vertical separation, where the tread of Q_{t5} conceals the strath of Q_{t3} in most locations

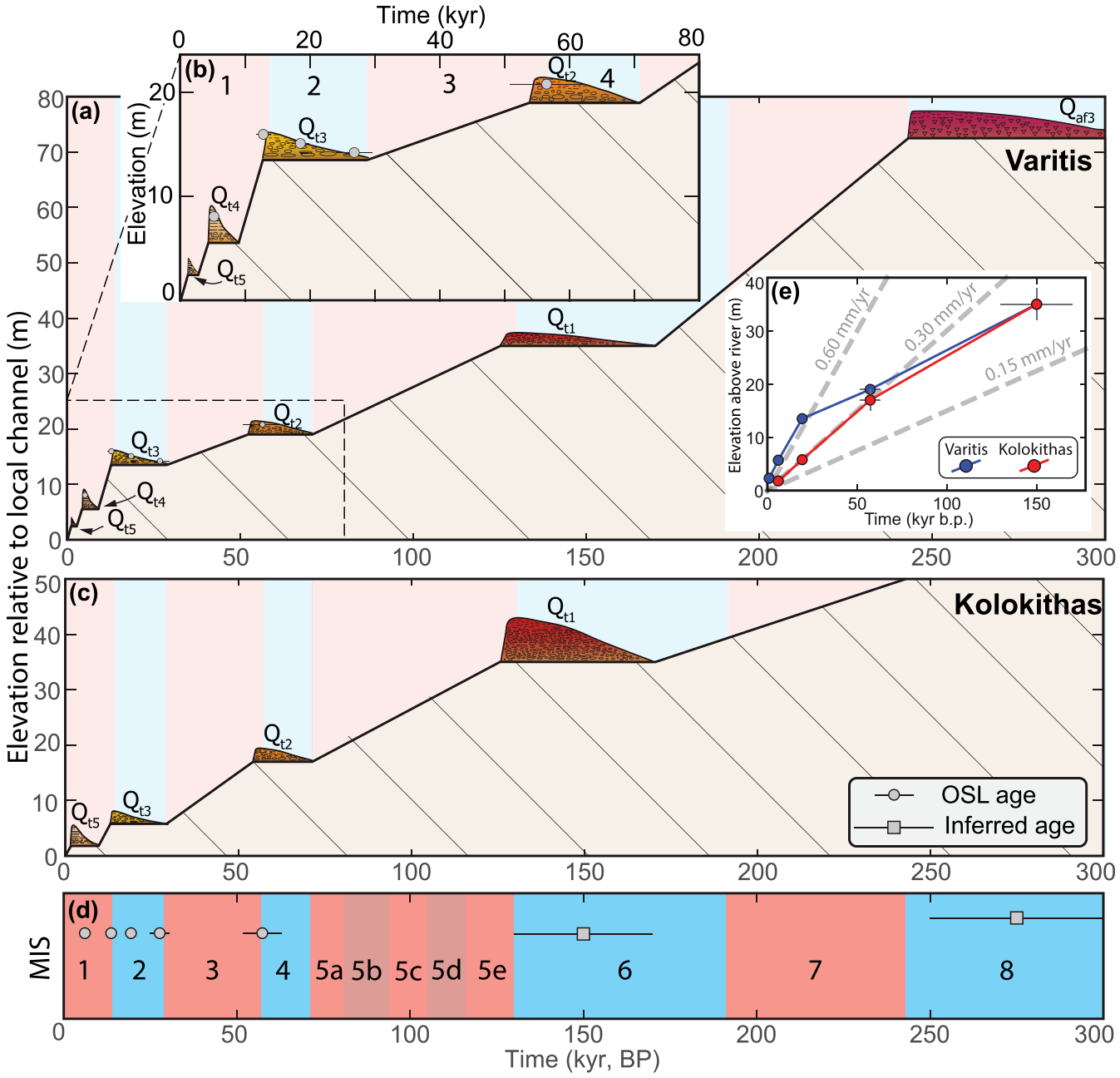

FIGURE 8 Conceptual model for aggradation versus incision history on the Varitis and Kolokithas Rivers and incision rates through time. The red and blue parts in Figure 8a–d show marine isotope states (MIS), where red relates to relatively warmer intervals, and blue indicates relatively cooler intervals. (a) Terrace genesis plot for the Varitis River. The grey dots show the age and elevation of optically stimulated luminescence (OSL) samples, and the horizontal bar shows the one standard deviation uncertainty. The dashed box shows the range shown in Figure 8b. (b) The same as Figure 8a but zooming in to show the younger terraces. (c) The same as in Figure 8a but for the Kolokithas River. (d) The relationship between OSL age or inferred deposit age where the horizontal bars represent one standard deviation uncertainty for the OSL and assumed uncertainties for inferred ages. (e) The incision rates for each river based on the average elevation of terrace units along each river.

(Figure 6). Furthermore, the Kolokithas Q_{t1} terrace is a ~8 m thick fill terrace, in contrast to the ~1–2 m thick Q_{t1} strath terrace on the Varitis River.

After the deposition of Q_{t1}, incision patterns diverge on the two rivers in a manner consistent with expectations for capture (Figure 7). On the Varitis River, as the captor, an increase in drainage area and water supply elevates stream power. The river responds by increasing incision rates upstream, producing the upstream-fanning incision pattern observed in the Varitis Valley (Figure 7d). In contrast, on the beheaded river, water supply reduction results in decreased incision rates in an upstream direction, which is what we see in Q_{t2} and Q_{t3} on the Kolokithas River (Figure 7a,c). These changes in water supply, and thus stream power, also provide a simple explanation for the changes in incision rate on the two rivers (Figure 8). The time-averaged rate on the Varitis, ~0.40 mm/year, is nearly double that on the Kolokithas, ~0.25 mm/year, since the inferred depositional timing of Q_{t1} (Figure 8e). Furthermore, while the Kolokithas incision rate is nearly steady over time, the Varitis rates increase to ~0.60 mm/year between ~50 and 25 kyr (Figure 8e). We do not see a change in average incision rate on the Kolokithas River, which is surprising. However, these results represent average incision rates across the entire valley. Incision rates slow locally on the Kolokithas moving upstream

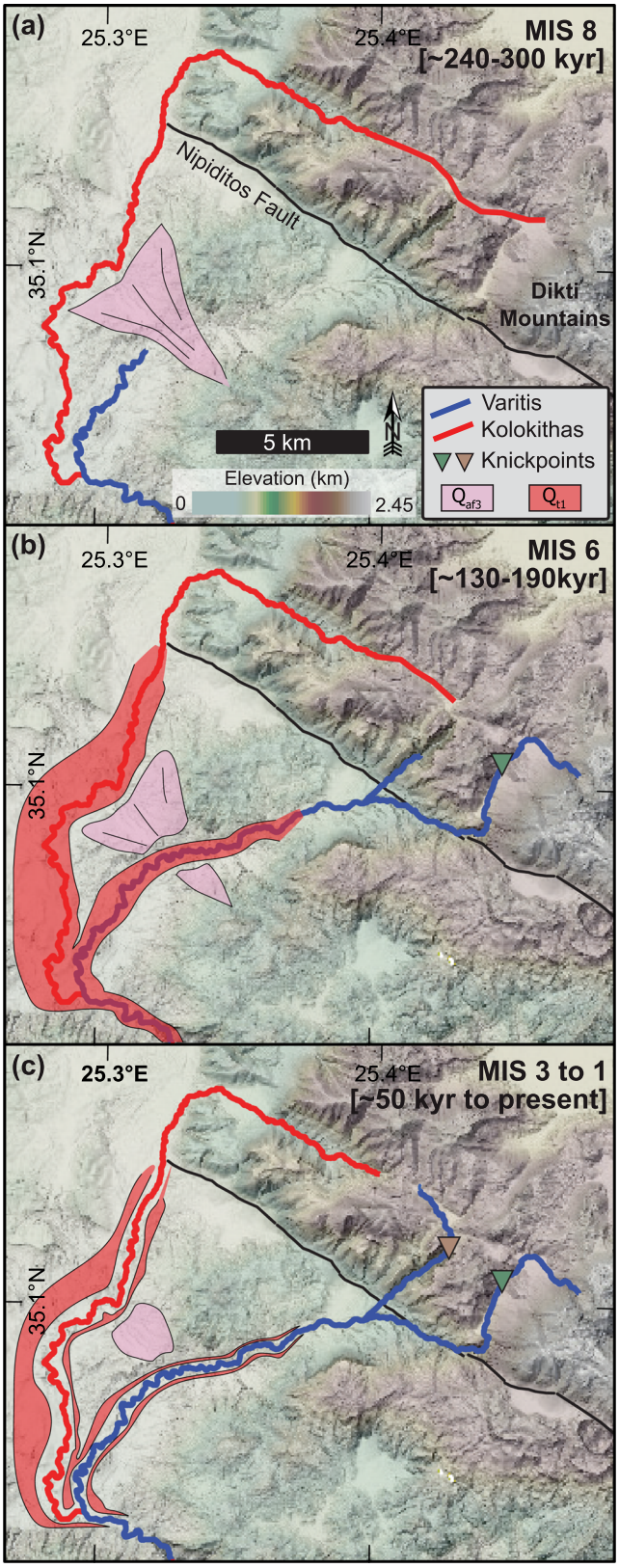

FIGURE 9 Map-view conceptual model illustrating the general history of capture as constrained by Quaternary deposits. (a) The Kolokithas drains the highest peaks in the Dikti Mountains. The Varitis is likely a small tributary that does not drain the high topography of the Dikti Mountains, as evidenced by the deposition of the Q_{af3} fan, sourced to the south and east of the modern drainage of the Varitis. (b) Q_{t1} is deposited as a fill terrace in the Kolokithas and a strath terrace on the Varitis. Q_{af3} is disconnected from the Dikti Mountains because of headward expansion and incision on the Varitis River, possibly because of slowing of the Nipiditos fault. It is inferred that the first capture occurred before the deposition of Q_{t1} (red polygon in Figure 9b and c). (c) A possible second capture occurred between ~50 and 25 kyr based on an increase in an incision rate on the Varitis evident in Q_{t3} and younger terraces (Figure 8e). This configuration persists to this day. For simplicity, not all Quaternary deposits are presented in this illustration.

for Q_{t2} and Q_{t3} as discussed earlier (Figure 7a,c), which aligns with expectations for a beheaded river. Interestingly, the long-term average incision rate of both valleys combined is similar to the coastal uplift rates at the river's outlet to the sea near Tsoutsourous of ~0.35 mm/year (Gallen et al., 2014; Gallen & Wegmann, 2017; Robertson et al., 2019). We suggest that the actively extending Messara Graben is uplifting at ~0.35 mm/year, and the higher and lower incision rates on the Varitis and Kolokithas Rivers, respectively, are because of the ongoing differential response to river capture.

Based on our geochronology and sedimentological and stratigraphic observations, we devise a conceptual model for terrace genesis and river incision in the Kolokithas and Varitis Rivers (Figure 8). The conceptual model envokes phases of valley aggradation during cooler periods, consistent with existing work on Crete and our geochronology (Figure 8). We note that the geochronology is not precise enough to definitively determine exactly when rivers transition from aggradation to incision or if there is a lag between Pleistocene terrace deposition and bedrock incision at climate transitions, given uncertainties on the OSL ages. However, the results consistently show deposition during cooler/wetter periods.

For the Pleistocene terraces, save for Q_{t1} on the Kolokithas, we infer long periods of lateral planation because of a thin (< 3 m) package of mobile alluvium (Figure 8). During transitions to warmer intervals, we envision incision commencing, allowing the accumulation of overbank material and later wind-blow sediment. The Holocene terraces are inferred to have been cut and aggregated over relatively shorter internals (Figure 8). We infer that the difference in Q_{t1} on the Kolokithas, a fill terrace, and the Varitis, a strath terrace, reflects the geomorphic legacy of river capture, which we discuss in more detail in the succeeding texts (Figures 5, 6 and 8).

5.4 | Landscape evolution history

We attribute the differences in terrace stratigraphy and incision rates on the Varitis and Kolokithas to river capture and beheading effects. Before ~150–250 kyr, we interpret the Varitis as a small river draining the Messara graben (Figure 9a). The Varitis must have been small at this time as it did not disrupt the deposition of Q_{af3} between the two rivers (Figures 4 and 9a). Before ~140 kyr, we infer the Varitis captured the Kolokithas headwaters, likely at the position of

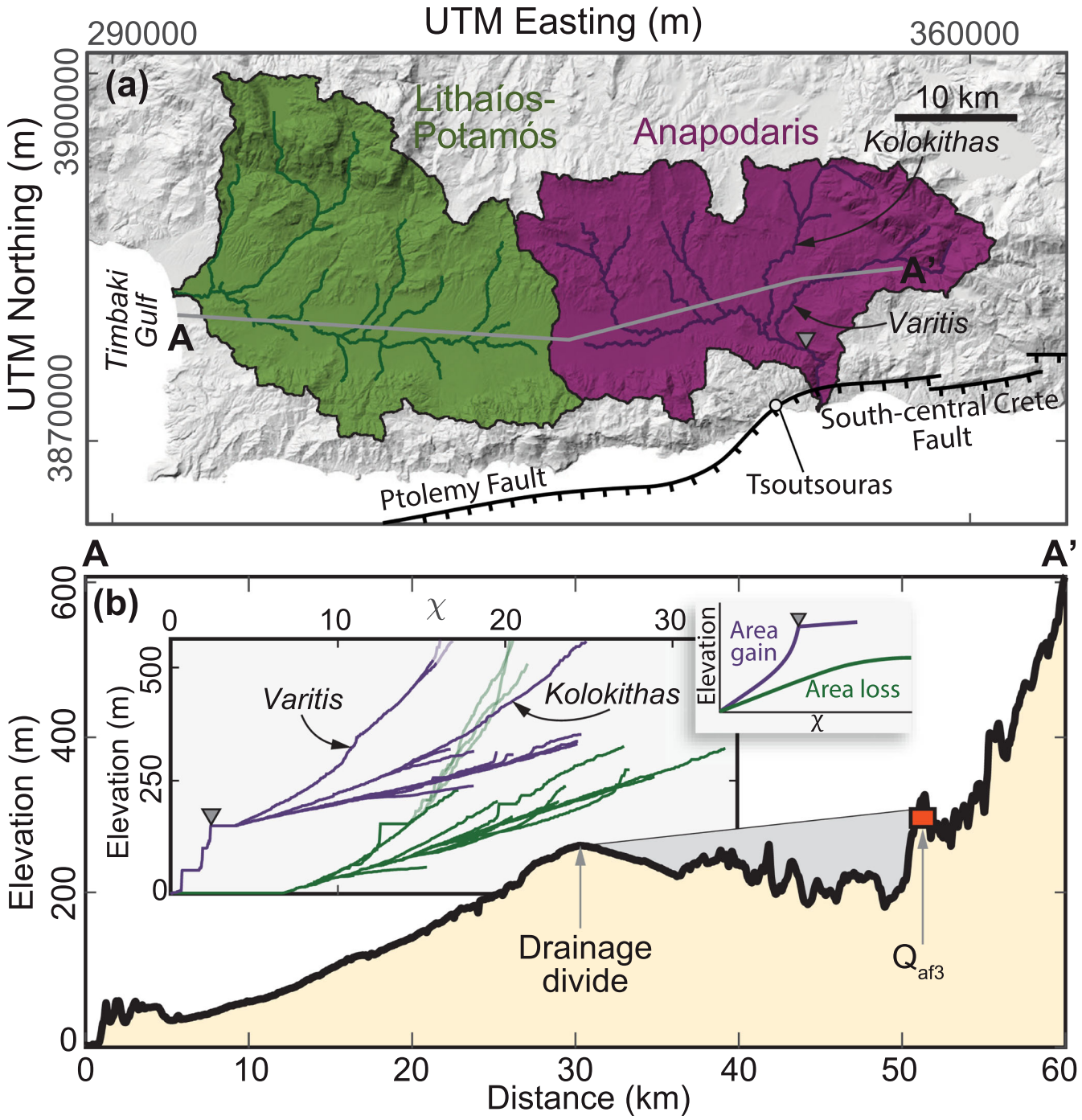

FIGURE 10 (a) Map showing the Lithaíos–Potamós (green) and Anapodaris (purple) drainage basins and rivers draining ≥10 km^2. The triangle shows the location of the knickpoint at the top of the Anapodaris gorge, as shown in the inset in Figure 10b. The black line shows the location of the topographic profile shown in Figure 10b. (b) Topographic profile highlighting the position of the main divide in relation to the Q_{af3} fan perched between the Varitis and Kolokithas Rivers. Not the incised, higher relief topography on the east side of the divide suggesting dissection in the Anapodaris drainage relative to the Lithaíos–Potamós drainage west of the divide. The inset shows χ-plots of the Lithaíos–Potamós (green) and Anapodaris (purple) stream network for rivers draining ≥10 km^2. The transparent river profile segments are in rocks that are not associated with sedimentary rock within the Messara graben. The knickpoint at the top of the Anapodaris gorge is denoted by the grey triangle. The leftward shift in the Anapodaris streams is consistent with interpretations of it capturing drainage area from the Lithaíos–Potamós and shown in the smaller inset cartoon.

the eastern knickpoint (Figure 9b), possibly because of waning activity of the Nipiditos Fault. The geomorphic response to this event included the enlargement and more rapid incision on the Varitis, allowing for the deposition of the Q_{t1} strath terrace. The reduction of water supply, but still substantial hillslope sediment supply, in the Kolokithas resulted in the deposition of the Q_{t1} fill terrace. We thus attribute the difference in the depositional character of Q_{t1} in each valley as the terrace record of river capture. Importantly, the lithologies underlying each basin are the same. There is no significant difference in rock type competence, either along the channel bed or as sedimentary clasts, that could account for the difference between one basin producing a strath terrace at the same time that the other

creates a fill terrace other than the lack of discharge in the Kolokithas necessary to transport the sediment delivered from hillslopes and tributaries (cf. Wegmann & Pazzaglia, 2009). We infer that a second capture, generating the more western knickpoint on the Varitis, occurred between ~50 and 25 kyr, based on the acceleration in incision rate on the Varitis (Figures 8 and 9c). We cannot confirm the interpretation, but it is reasonable given the data. Since ~25 kyr, the drainage configuration in the Anapodaris drainage basin has remained roughly the same (Figure 9c). Importantly, despite the impact of drainage reorganisation, climate paces terrace aggradation and incision during the Pleistocene.

More broadly, it is likely that the drainage area changes and transient river system dynamics reported in this study result from an ongoing larger-scale reorganisation of the Messara Graben drainage system. The ~520 km^2 Anapodaris and 600 km^2 Lithaíos–Potamós river systems drain the eastern and western portions of the Messara, respectively (Figure 10a). Both drainage basins are of comparable size and share a common drainage divide at ~260 m near the centre of the Messara graben (Figure 10b). The Lithaíos–Potamós maintains a low gradient throughout the Messara to the Timbaki Gulf, while the Anapodaris spills out to the Mediterranean through a steep and narrow gorge (Figure 10b, inset). χ-plots of these two rivers show distortions possibly consistent with the recent capture of a previously much larger Lithaíos–Potamós drainage system by the Anapodaris (Figure 10b, inset). In this interpretation, the paleo-Lithaíos–Potamós river would have stretched across the Messara and drained the Dikti Mountains. The top of the steep Anapodaris Gorge marks the approximate location where the capture occurred. The modern drainage divide between the Anapodaris and Lithaíos–Potamós drainage basins is ~40 m lower than the large Q_{af3} fan mapped between the Varitis and Kolokithas Rivers (Figures 4 and 10a). It is, therefore, possible that Q_{af3} was deposited when the local base level was higher and set by the paleo-Lithaíos–Potamós rather than the lower base level imposed by the Anapodaris today.

If correct, this hypothesis suggests that the establishment of the east–west drainage divide in the Messara occurred after the deposition of the Q_{af3} fan (post-MIS 8). The Anapodaris River Gorge is carved across the footwall uplift of the now hard-linked South Central Crete and Ptolemy faults (Gallen et al., 2014; Figure 10a). Fault linkage causes increased footwall slip and uplift rates across the linkage zone (Dawers & Anders, 1995) as the combined longer fault reestablishes a more geometrically preferred fault aspect ratio (a fault's strike length to down-dip length). Based on nearby coastal (marine terrace) uplift rates, hard linkage of the two faults likely occurred during or after MIS 9 and certainly before MIS 7 (ca. 210–330 ka; Gallen et al., 2014). The Q_{t1} terrace in this study post-dates the capture of the upper portions of the Lithaíos–Potamós River by the Anapodaris River. If our age assignment for Q_{t1} of MIS 6 is correct, the capture and drainage rearrangement and integration within the eastern Mesara graben likely happened during or after MIS 8 and certainly before the end of MIS 7. This hypothesis is testable by studying sediments in the Timbaki Gulf and offshore of the Anapodaris River.

5.5 | General implications

This study demonstrates that river capture can affect river terrace stratigraphy, incision rates and patterns. These findings contribute to a collection of research emphasising the importance of other geomorphic processes that can affect sediment and water supply when interpreting river terraces as tectonic and climate records (Finnegan & Dietrich, 2011; García, 2006; García & Mahan, 2014; Limaye & Lamb, 2016; Maher, Harvey, & France, 2007; Pederson et al., 2024; Stokes & Mather, 2000; Stokes, Mather, & Harvey, 2002; Whitfield & Harvey, 2012). The Varitis and Kolokithas river terrace records indicate that phases of Pleistocene fluvial aggradation and incision are paced by Quaternary climate change, with aggradation common during cooler intervals, consistent with previous studies on Crete (Ott et al., 2023; Pope et al., 2008; Pope, Candy, & Skourtsos, 2016). However, differences in terrace characteristics (e.g. fill vs strath terrace) and incision rates and patterns are dictated by the legacy of river capture. The average incision rate considering both rivers is consistent with the coastal uplift rate at the river outlet, implying that tectonically driven rock uplift dictates base-level lowering rates. These results indicate that Pleistocene-scale climate and tectonic signals are preserved in the Anapodaris and Varitis River systems; however, direct interpretations of these climate and tectonics are complicated by the ongoing response to capture. Care should be taken when drawing interpretations from river terraces regarding climate and tectonics when only studying a single river valley.

6 | CONCLUSIONS AND SUMMARY

This study presents a detailed analysis of the Pleistocene river terrace and bedrock incision response to capture and beheading two rivers that share a confluence. Our results show differences in terrace stratigraphy, the number of terraces and river incision rates among the two rivers. Geochronology shows that terrace genesis is linked to Quaternary climate change during the Pleistocene, with aggradation occurring during cooler periods, consistent with past work. Holocene terraces are interpreted to result from anthropogenic landscape change and soil erosion, possibly modulated by Holocene climate dynamics. Our results suggest that river discharge changes best explain terrace characteristics and incision rates on the Varitis and Kolokithas Rivers. Reductions in discharge on the beheaded Kolokithas can explain the deposition of a large fill terrace near the inferred time of capture and, subsequently, slower incision rates relative to the Varitis. Collectively, our study shows that the terraces on the Varitis and Kolokithas Rivers reflect climate and tectonic forcings; however, important differences in terrace stratigraphy and incision rate and patterns are related to the ongoing response to capture cloud direct interpretation of river terraces as climate and tectonic records. We conclude that river capture can be important in affecting river terrace genesis and bedrock incision rates. Fluvial systems are still sensitive to climate and tectonic processes even when affected by drainage reorganisation. Still, direct interpretations are more challenging in systems perturbed by dynamic drainage processes, such as river capture.

AUTHOR CONTRIBUTIONS

Sean F. Gallen and Karl W. Wegmann conceived the study and participated in fieldwork. Sean F. Gallen conducted the mapping, sedimentological and soil descriptions, geochronological sampling, map digitisation, and topographic analysis and drafted the initial version of

the figures and text with input from Karl W. Wegmann. Sean F. Gallen and Karl W. Wegmann worked jointly to edit and revise the analyses, figures and text.

ACKNOWLEDGEMENTS

The authors thank financial support from the Donors of the American Chemical Society Petroleum Research Fund grant #50792-DNI8 to Wegmann and a 2011 Geological Society of America Graduate Student Research Grant (number 9596-11), a 2012 Sigma Xi Grant-in-Aid of Research, NSF-Tectonics award #2041910, and NSF-Geomorphology and Land-use Dynamics award #2139894 to Gallen. We acknowledge the Greek Institute of Geology and Mineral Exploration for granting permission to conduct fieldwork on Crete. We thank Hellenic Cadastre SA for access to the DTM data. We are indebted to Charalampos Fassoulas and Nikos Somarakis for logistical and moral support while in the field. The authors also thank two anonymous reviewers and editor, Stuart Lane, for constructive feedback that helped improve this manuscript.

CONFLICT OF INTEREST STATEMENT

We declare no conflicts of interest.

DATA AVAILABILITY STATEMENT

The digital topographic data used in this study are available by request from the Hellenic Cadastre SA. A shapefile of the Quaternary map units is archived as a citable data set in Dryad at the following DOI: https://doi.org/10.5061/dryad.8gtht7709. These new data have not been previously published and are not under consideration for publication anywhere else.

ORCID

Sean F. Gallen https://orcid.org/0000-0002-9288-2850

REFERENCES

Angelier, J., Lybéris, N., Le Pichon, X., Barrier, E. & Huchon, P. (1982) The tectonic development of the Hellenic arc and the sea of Crete: a synthesis. *Tectonophysics*, 86(1), 159–196. Available from: https://doi.org/10.1016/0040-1951(82)90066-X

Benito, G., Macklin, M.G., Zielhofer, C., Jones, A.F. & Machado, M.J. (2015) Holocene flooding and climate change in the Mediterranean. *Catena*, 130, 13–33. Available from: https://doi.org/10.1016/j.catena.2014.11.014

Bruni, E.T., Ott, R.F., Picotti, V., Haghipour, N., Wegmann, K.W. & Gallen, S.F. (2021) Stochastic alluvial fan and terrace formation triggered by a high-magnitude Holocene landslide in the Klados gorge, Crete. *Earth Surface Dynamics*, 9(4), 771–793. Available from: https://doi.org/10.5194/esurf-9-771-2021

Bucher, W.H. (1932) "Strath" as a geomorphic term. *Science*, 75(1935), 130–131. Available from: https://doi.org/10.1126/science.75.1935.130.b

Bull, W.B. (1991) *Geomorphic responses to climatic change*. New York: Oxford University Press.

Caputo, R., Catalano, S., Monaco, C., Romagnoli, G., Tortorici, G. & Tortorici, L. (2010) Active faulting on the island of Crete (Greece). *Geophysical Journal International*, 183(1), 111–126. Available from: https://doi.org/10.1111/j.1365-246X.2010.04749.x

Coltorti, M. & Dramis, F. (1995) The chronology of Upper Pleistocene stratified slope-waste deposits in Central Italy. *Permafrost and Periglacial Processes*, 6(3), 235–242. Available from: https://doi.org/10.1002/ppp.3430060304

Dawers, N.H. & Anders, M.H. (1995) Displacement-length scaling and fault linkage. *Journal of Structural Geology*, 17(5), 607–614. Available from: https://doi.org/10.1016/0191-8141(94)00091-D

Dusar, B., Verstraeten, G., Notebaert, B. & Bakker, J. (2011) Holocene environmental change and its impact on sediment dynamics in the eastern Mediterranean. *Earth-Science Reviews*, 108(3), 137–157. Available from: https://doi.org/10.1016/j.earscirev.2011.06.006

Finnegan, N.J. & Dietrich, W.E. (2011) Episodic bedrock strath terrace formation due to meander migration and cutoff. *Geology*, 39(2), 143–146. Available from: https://doi.org/10.1130/G31716.1

Flint, J.J. (1974) Stream gradient as a function of order, magnitude, and discharge. *Water Resources Research*, 10(5), 969–973. Available from: https://doi.org/10.1029/WR010i005p00969

Gallen, S.F. (2018) Lithologic controls on landscape dynamics and aquatic species evolution in post-orogenic mountains. *Earth and Planetary Science Letters*, 493, 150–160. Available from: https://doi.org/10.1016/j.epsl.2018.04.029

Gallen, S.F. & Thigpen, J.R. (2018) Lithologic controls on focused erosion and intraplate earthquakes in the eastern Tennessee seismic zone. *Geophysical Research Letters*, 45(18), 9569–9578. Available from: https://doi.org/10.1029/2018GL079157

Gallen, S.F. & Wegmann, K.W. (2017) River profile response to normal fault growth and linkage: an example from the Hellenic forearc of south-central Crete, Greece. *Earth Surface Dynamics*, 5(1), 161–186. Available from: https://doi.org/10.5194/esurf-5-161-2017

Gallen, S.F., Pazzaglia, F.J., Wegmann, K.W., Pederson, J.L. & Gardner, T.W. (2015) The dynamic reference frame of rivers and apparent transience in incision rates. *Geology*, 43(7), 623–626. Available from: https://doi.org/10.1130/G36692.1

Gallen, S.F., Wegmann, K.W., Bohnenstiehl, D.R., Pazzaglia, F.J., Brandon, M.T. & Fassoulas, C. (2014) Active simultaneous uplift and margin-normal extension in a forearc high, Crete, Greece. *Earth and Planetary Science Letters*, 398, 11–24. Available from: https://doi.org/10.1016/j.epsl.2014.04.038

García, A.F. (2006) Thresholds of strath genesis deduced from landscape response to stream piracy by Pancho Rico creek in the coast ranges of Central California. *American Journal of Science*, 306(8), 655–681. Available from: https://doi.org/10.2475/08.2006.03

García, A.F. & Mahan, S.A. (2014) The notion of climate-driven strath-terrace production assessed via dissimilar stream-process response to Late Quaternary climate. *Geomorphology*, 214, 223–244. Available from: https://doi.org/10.1016/j.geomorph.2014.02.008

Giachetta, E. & Willett, S.D. (2018) Effects of river capture and sediment flux on the evolution of plateaus: insights from numerical modeling and river profile analysis in the upper Blue Nile catchment. *Journal of Geophysical Research: Earth Surface*, 123(6), 1187–1217. Available from: https://doi.org/10.1029/2017JF004252

Harel, E., Goren, L., Shelef, E. & Ginat, H. (2019) Drainage reversal toward cliffs induced by lateral lithologic differences. *Geology*, 47(10), 928–932. Available from: https://doi.org/10.1130/G46353.1

Harvey, A.M., Whitfield (nee Maher), E., Stokes, M. & Mather, A. (2014) The late neogene to quaternary drainage evolution of the uplifted neogene sedimentary basins of Almería, Betic Chain. In: Gutiérrez, F. & Gutiérrez, M. (Eds.), *Landscapes and landforms of Spain*. Dordrecht, Netherlands: Springer, pp. 37–61. Available from: https://doi.org/10.1007/978-94-017-8628-7_3

Jolivet, L. & Brun, J.-P. (2010) Cenozoic geodynamic evolution of the Aegean. *International Journal of Earth Sciences*, 99(1), 109–138. Available from: https://doi.org/10.1007/s00531-008-0366-4

Jouffroy-Bapicot, I., Pedrotta, T., Debret, M., Field, S., Sulpizio, R., Zanchetta, G., et al. (2021) Olive groves around the lake. A ten-thousand-year history of a Cretan landscape (Greece) reveals the dominant role of humans in making this Mediterranean ecosystem. *Quaternary Science Reviews*, 267, 107072. Available from: https://doi.org/10.1016/j.quascirev.2021.107072

Lavé, J. & Avouac, J.P. (2000) Active folding of fluvial terraces across the Siwaliks Hills, Himalayas of Central Nepal. *Journal of Geophysical Research: Solid Earth*, 105(B3), 5735–5770. Available from: https://doi.org/10.1029/1999JB900292

Lavé, J. & Avouac, J.P. (2001) Fluvial incision and tectonic uplift across the Himalayas of Central Nepal. *Journal of Geophysical Research: Solid Earth*, 106(B11), 26561–26591. Available from: https://doi.org/10.1029/2001JB000359

Limaye, A.B.S. & Lamb, M.P. (2016) Numerical model predictions of autogenic fluvial terraces and comparison to climate change expectations. *Journal of Geophysical Research: Earth Surface*, 121(3), 512–544. Available from: https://doi.org/10.1002/2014JF003392

Macklin, M.G., Fuller, I.C., Lewin, J., Maas, G.S., Passmore, D.G., Rose, J., et al. (2002) Correlation of fluvial sequences in the Mediterranean basin over the last 200 ka and their relationship to climate change. *Quaternary Science Reviews*, 21(14), 1633–1641. Available from: https://doi.org/10.1016/S0277-3791(01)00147-0

Macklin, M.G., Tooth, S., Brewer, P.A., Noble, P.L. & Duller, G.A.T. (2010) Holocene flooding and river development in a Mediterranean steepland catchment: the Anapodaris gorge, south central Crete, Greece. *Global and Planetary Change*, 70(1), 35–52. Available from: https://doi.org/10.1016/j.gloplacha.2009.11.006

Maher, E., Harvey, A.M. & France, D. (2007) The impact of a major Quaternary river capture on the alluvial sediments of a beheaded river system, the Rio alias, SE Spain. *Geomorphology*, 84(3), 344–356. Available from: https://doi.org/10.1016/j.geomorph.2005.07.034

Marder, E., Gallen, S.F. & Pazzaglia, F.J. (2023) Late Cenozoic deformation in the U.S. southern Colorado front range revealed by river profile analysis and fluvial terraces. *Geological Society of America Bulletin*, 136(3–4), 1067–1085. Available from: https://doi.org/10.1130/B36440.1

Mather, A.E. (2000) Impact of headwater river capture on alluvial system development: an example from the Plio-Pleistocene of the Sorbas Basin, SE Spain. *Journal of the Geological Society*, 157(5), 957–966. Available from: https://doi.org/10.1144/jgs.157.5.957

Meulenkamp, J.E., van der Zwaan, G.J. & van Wamel, W.A. (1994) On late Miocene to recent vertical motions in the Cretan segment of the Hellenic arc. *Tectonophysics*, 234(1), 53–72. Available from: https://doi.org/10.1016/0040-1951(94)90204-6

Nemec, W. & Postma, G. (1993) Quaternary alluvial fans in southwestern Crete: sedimentation processes and geomorphic evolution. In: *Alluvial sedimentation*. Oxford, UK: Blackwell Publishing Ltd, pp. 235–276 https://doi.org/10.1002/9781444303995.ch18

Nicol, A., Mouslopoulou, V., Begg, J. & Oncken, O. (2020) Displacement accumulation and sampling of paleoearthquakes on active normal faults of Crete in the eastern mediterranean. *Geochemistry, Geophysics, Geosystems*, 21(11), e2020GC009265. Available from: https://doi.org/10.1029/2020GC009265

Ott, R.F., Gallen, S.F., Caves Rugenstein, J.K., Ivy-Ochs, S., Helman, D., Fassoulas, C., et al. (2019a) Chemical versus mechanical denudation in meta-clastic and carbonate bedrock catchments on Crete, Greece, and mechanisms for steep and high carbonate topography. *Journal of Geophysical Research: Earth Surface*, 124(12), 2943–2961. Available from: https://doi.org/10.1029/2019JF005142

Ott, R.F., Gallen, S.F., Wegmann, K.W., Biswas, R.H., Herman, F. & Willett, S.D. (2019b) Pleistocene terrace formation, quaternary rock uplift rates and geodynamics of the hellenic subduction zone revealed from dating of paleoshorelines on Crete, Greece. *Earth and Planetary Science Letters*, 525, 115757. Available from: https://doi.org/10.1016/j.epsl.2019.115757

Ott, R.F., Scherler, D., Wegmann, K.W., D'Arcy, M.K., Pope, R.J., Ivy-Ochs, S., et al. (2023) Paleo-denudation rates suggest variations in runoff drove aggradation during last glacial cycle, Crete, Greece. *Earth Surface Processes and Landforms*, 48(2), 386–405. Available from: https://doi.org/10.1002/esp.5492

Pazzaglia, F.J. (2022) 6.32 - Fluvial Terraces. In: Shroder, J.(J.)F. (Ed.) *Treatise on geomorphology*, Second edition. Oxford: Academic Press, pp. 639–679 https://doi.org/10.1016/B978-0-12-409548-9.12088-3

Pazzaglia, F.J. & Brandon, M.T. (2001) A fluvial record of long-term steady-state uplift and erosion across the Cascadia forearc high, western Washington state. *American Journal of Science*, 301(4–5), 385–431. Available from: https://doi.org/10.2475/ajs.301.4-5.385

Pederson, J.L., Young, S.C., Turley, M., Tanski, N., Rittenour, T.M. & Harris, R.A. (2024) The how, when, and why of an abandoned bedrock meander of the Colorado River, Utah (U.S.). *Earth Surface Processes and Landforms*, 49(11), 1–9. Available from: https://doi.org/10.1002/esp.5886

Perron, J.T. & Royden, L. (2013) An integral approach to bedrock river profile analysis. *Earth Surface Processes and Landforms*, 38(6), 570–576. Available from: https://doi.org/10.1002/esp.3302

Peterek, A. & Schwarze, J. (2004) Architecture and late Pliocene to recent evolution of outer-arc basins of the Hellenic subduction zone (south-central Crete, Greece). *Journal of Geodynamics*, 38(1), 19–55. Available from: https://doi.org/10.1016/j.jog.2004.03.002

Pope, R., Wilkinson, K., Skourtsos, E., Triantaphyllou, M. & Ferrier, G. (2008) Clarifying stages of alluvial fan evolution along the Sfakian piedmont, southern Crete: new evidence from analysis of post-incisive soils and OSL dating. *Geomorphology*, 94(1), 206–225. Available from: https://doi.org/10.1016/j.geomorph.2007.05.007

Pope, R.J.J., Candy, I. & Skourtsos, E. (2016) A chronology of alluvial fan response to Late Quaternary sea level and climate change, Crete. *Quaternary Research*, 86(2), 170–183. Available from: https://doi.org/10.1016/j.yqres.2016.06.003

Rackham, O. & Moody, J. (1997) *The making of the Cretan landscape*, First edition. Manchester, UK: Manchester University Press 237 p.

Reilinger, R., McClusky, S., Paradissis, D., Ergintav, S. & Vernant, P. (2010) Geodetic constraints on the tectonic evolution of the Aegean region and strain accumulation along the Hellenic subduction zone. *Tectonophysics*, 488(1), 22–30. Available from: https://doi.org/10.1016/j.tecto.2009.05.027

Reilinger, R., McClusky, S., Vernant, P., Lawrence, S., Ergintav, S., Cakmak, R., et al. (2006) GPS constraints on continental deformation in the Africa-Arabia-Eurasia continental collision zone and implications for the dynamics of plate interactions. *Journal of Geophysical Research: Solid Earth*, 111(B5), B05411. Available from: https://doi.org/10.1029/2005JB004051

Rhodes, E.J. (2011) Optically stimulated luminescence dating of sediments over the past 200,000 years. *Annual Review of Earth and Planetary Sciences*, 39, 461–488. Available from: https://doi.org/10.1146/annurev-earth-040610-133425

Robertson, J., Meschis, M., Roberts, G.P., Ganas, A. & Gheorghiu, D.M. (2019) Temporally constant quaternary uplift rates and their relationship with extensional upper-plate faults in South Crete (Greece), constrained with ^{36}Cl cosmogenic exposure dating. *Tectonics*, 38(4), 1189–1222. Available from: https://doi.org/10.1029/2018TC005410

Robertson, J., Roberts, G.P., Ganas, A., Meschis, M., Gheorghiu, D.M. & Shanks, R.P. (2023) Quaternary uplift of palaeoshorelines in southwestern Crete: the combined effect of extensional and compressional faulting. *Quaternary Science Reviews*, 316, 108240. Available from: https://doi.org/10.1016/j.quascirev.2023.108240

Rose, J., Meng, X. & Watson, C. (1999) Palaeoclimate and palaeoenvironmental responses in the western Mediterranean over the last 140 ka: evidence from Mallorca, Spain. *Journal of the Geological Society*, 156(2), 435–448. Available from: https://doi.org/10.1144/gsjgs.156.2.0435

Runnels, C., DiGregorio, C., Wegmann, K.W., Gallen, S.F., Strasser, T.F. & Panagopoulou, E. (2014) Lower palaeolithic artifacts from Plakias, Crete: implications for hominin dispersals. *Eurasian Prehistory*, 11(1–2), 129–152.

Scheingross, J.S., Limaye, A.B., McCoy, S.W. & Whittaker, A.C. (2020) The shaping of erosional landscapes by internal dynamics. *Nature Reviews Earth & Environment*, 1(12), 661–676. Available from: https://doi.org/10.1038/s43017-020-0096-0

Scherler, D., Lamb, M.P., Rhodes, E.J. & Avouac, J.-P. (2016) Climate-change versus landslide origin of fill terraces in a rapidly eroding bedrock landscape: San Gabriel River, California. *GSA Bulletin*, 128(7–8), 1228–1248. Available from: https://doi.org/10.1130/B31356.1

Schumm, S.A. (1969) River metamorphosis. *Journal of the Hydraulics Division*, 95(1), 255–274. Available from: https://doi.org/10.1061/JYCEAJ.0001938

Schwanghart, W. & Scherler, D. (2014) Short communication: topotoolbox 2 – MATLAB-based software for topographic analysis and modeling in earth surface sciences. *Earth Surface Dynamics*, 2(1), 1–7. Available from: https://doi.org/10.5194/esurf-2-1-2014

Schwanghart, W. & Scherler, D. (2017) Bumps in river profiles: uncertainty assessment and smoothing using quantile regression techniques. *Earth Surface Dynamics*, 5(4), 821–839. Available from: https://doi.org/10.5194/esurf-5-821-2017

Stokes, M. & Mather, A.E. (2000) Response of Plio-Pleistocene alluvial systems to tectonically induced base-level changes, vera basin, SE Spain. *Journal of the Geological Society*, 157(2), 303–316. Available from: https://doi.org/10.1144/jgs.157.2.303

Stokes, M., Mather, A.E. & Harvey, A.M. (2002) Quantification of river-capture-induced base-level changes and landscape development, Sorbas basin, SE Spain. *Geological Society, London, Special Publications*, 191(1), 23–35. Available from: https://doi.org/10.1144/GSL.SP.2002.191.01.03

van Hinsbergen, D.J.J. & Meulenkamp, J.E. (2006) Neogene supradetachment basin development on Crete (Greece) during exhumation of the South Aegean core complex. *Basin Research*, 18(1), 103–124. Available from: https://doi.org/10.1111/j.1365–2117.2005.00282.x

Vernant, P., Reilinger, R. & McClusky, S. (2014) Geodetic evidence for low coupling on the Hellenic subduction plate interface. *Earth and Planetary Science Letters*, 385, 122–129. Available from: https://doi.org/10.1016/j.epsl.2013.10.018

Wegmann, K. (2008) *Tectonic geomorphology above Mediterranean subduction zones: northeastern Apennines of Italy and Crete, Greece (Ph.D.)*. United States -- Pennsylvania: Lehigh University Retrieved from https://www.proquest.com/docview/304563344/abstract/13A452E57F4D4183PQ/1

Wegmann, K.W. & Gallen, S.F. (2022) 2.06 - Tectonic geomorphology above Mediterranean subduction zones. In: Shroder, J.(J.)F. (Ed.) *Treatise on geomorphology*, Second edition. Oxford: Academic Press, pp. 87–119 https://doi.org/10.1016/B978-0-12-818234-5.00223–6

Wegmann, K.W. & Pazzaglia, F.J. (2002) Holocene strath terraces, climate change, and active tectonics: the Clearwater River basin, Olympic peninsula, Washington state. *GSA Bulletin*, 114(6), 731–744. Available from: https://doi.org/10.1130/0016–7606(2002)114<0731:HSTCCA>2.0.CO;2

Wegmann, K.W. & Pazzaglia, F.J. (2009) Late Quaternary fluvial terraces of the Romagna and Marche Apennines, Italy: climatic, lithologic, and tectonic controls on terrace genesis in an active orogen. *Quaternary Science Reviews*, 28(1), 137–165. Available from: https://doi.org/10.1016/j.quascirev.2008.10.006

Whitfield, E. & Harvey, A.M. (2012) Interaction between the controls on fluvial system development: tectonics, climate, base level and river capture – Rio Alias, Southeast Spain. *Earth Surface Processes and Landforms*, 37(13), 1387–1397. Available from: https://doi.org/10.1002/esp.3247

Willett, S.D., McCoy, S.W., Perron, J.T., Goren, L. & Chen, C.-Y. (2014) Dynamic reorganization of river basins. *Science*, 343(6175), 1248765. Available from: https://doi.org/10.1126/science.1248765

Zachariasse, W.J., van Hinsbergen, D.J.J. & Fortuin, A.R. (2008) Mass wasting and uplift on Crete and Karpathos during the early Pliocene related to initiation of South Aegean left-lateral, strike-slip tectonics. *GSA Bulletin*, 120(7–8), 976–993. Available from: https://doi.org/10.1130/B26175.1

SUPPORTING INFORMATION

Additional supporting information can be found online in the Supporting Information section at the end of this article.

How to cite this article: Gallen, S.F. & Wegmann, K.W. (2025) The impact of river capture on fluvial terraces and bedrock incision. *Earth Surface Processes and Landforms*, 50(3), e70035. Available from: https://doi.org/10.1002/esp.70035

Supplementary Materials for:

The impact of river capture on fluvial terraces and bedrock incision

Description: This file contains a table of luminescence geochronology results, extended methods on the luminescence geochronology, and detailed soil profile descriptions for select Pleistocene terraces and alluvial fans.

OSL dating report for Varitis River, Crete, Greece:

Quartz OSL dating results

Field ID	Latitude	Longitude	Terrace	Lab No	K	U	Th	Moisture	Size	Depth	Dose Rate	Equivalent Dose	Age
					%	ppm	ppm	%	µm	m	Gy/Kyr	Gy (mean ± 1 σ_s)	Kyr
sfg-050512-1	35.0386	25.2938	Q_{t3}	LS1363	0.95	1.3	6.33	15+/-5	90-125	1	1.573 ± 0.09	21.51 ± 1.13	13.676 ± 1.13
sfg-050712-1	35.0480	25.2914	Q_{t2}	LS1364	1.42	0.8	3.5	15+/-5	90-125	1.5	1.669 ± 0.111	10.18 ± 0.51	6.098 ± 0.537
sfg-050812-1	35.0680	25.3104	Q_{t3}	LS1365	0.94	1.56	3.21	15+/-5	90-125	1.5	1.425 ± 0.084	27.57 ± 1.54	19.348 ± 1.25
sfg-051312-1	35.0876	25.3686	Q_{t3}	LS1366	1.74	0.9	6.3	15+/-5	90-125	2	2.123 ± 0.138	58.81 ± 2.17	27.697 ± 2.84
sfg-051612-1	35.0487	25.2907	Q_{t4}	LS1367	0.82	0.73	2.6	15+/-5	90-125	2	1.117 ± 0.069	64.03 ± 2.28	57.318 ± 5.636

Sample preparation

For each sample, pure quartz was extracted for De measurements. In the OSL lab, the sample was treated firstly with 10% HCl and 30% H_2O_2 to remove organic materials and carbonates, respectively. After grain size separation, the 90-125 µm fraction was relatively abundant. As a result, this fraction was chosen for De determination. The grains were treated with HF acid (40%) for about 35 min, followed by 10% HCl acid to remove fluoride precipitates.

Measurement techniques

Quartz OSL measurements were performed using an automated Risø TL/OSL-20 reader. Stimulation was carried out by a blue LED (λ=470 ± 20 nm) stimulation source for 40 s at 130° C. Irradiation was carried out using a $^{90}Sr/^{90}Y$ beta source built into the reader. The OSL signal was detected by a 9235QA photomultiplier tube through a U-340 filter with 7.5 mm thickness.

Equivalent dose (De) measurement and age calculation

For De determination, the SAR protocol was adopted using a preheat temperature of 260° C for 10 s and a cut-heat temperature of 180° C for 10 s. The final De is the average De of all aliquots, and the error of the final De is the standard error of the De distribution. For each sample, 20–25 aliquots were measured for De determination.

The Quartz OSL was fast component-dominated. Recycling ratios were between 0.90 and 1.1. Recuperation is negligible. The cosmic ray dose rate was estimated for each sample as a function of depth, altitude, and geomagnetic latitude. The concentration of U, Th, and K was measured by ICP-MS. The elemental concentrations were then converted into annual dose rates, taking into account the estimated water content effect. The final OSL age is then De/dose rate.

Anapodaris Drainage Basins Quaternary Deposit Soil Profile Descriptions

Location: North of Kato Kastastili. GPS → N: 35.03861, E: 025.93814. Elevation: 169.3m

Soil developed on a $\mathbf{Q_{t3}}$ alluvial terrace. The upper horizons are matrix-supported, and the lower horizons are clast-supported. Clasts are many and predominantly rounded medium to large limestone with some chert, sandstone, phyllite, and random quartz. The slope is southwest-facing and has a 0–6% grade. It is well drained and has a Xeric moisture regime.

Ap (0 – 25 cm): 2.5Y 6/4 light yellowish brown clay loam. Moderate, fine subangular blocky structure. Very friable, slightly sticky, non-plastic consistency. Round clasts are common. Abrupt smooth boundary.
E (25 – 41cm): 2.5Y 7/3 pale yellow clay loam. Weak, fine, subangular blocky structure. Very friable, non-sticky, non-plastic consistency. Round clasts are common—clear, smooth boundary.
Bk (41 – 113cm): 10YR 5/4 yellowish brown, sandy clay loam. Moderate, medium, subangular block structure. Friable, sticky, slightly plastic consistency. Common coarse clasts. Gradual wavy boundary.
Bw (113-160cm): 10YR 6/6 brownish yellow, sandy clay loam. Weak, medium subangular block structure. Friable, slightly sticky, slightly plastic consistency. Common coarse clasts. Clear, wavy boundary.
C (>160cm): 10 YR 6/6 brownish yellow, sandy clay loam. Weak, medium subangular block structure. Friable, slightly sticky, slightly plastic consistency. Many coarse clasts.

Location: North of Kato Kastastili. GPS → N: 35.03818, E: 025.27232. Elevation: 192.7m

Soil developed on a $\mathbf{Q_{t1}}$ alluvial terrace. The upper horizons are matrix-supported, and the lower horizons are clast-supported. Clasts are many and predominantly rounded medium to large limestone with some chert, sandstone, phyllite, and random quartz. The slope is south-facing and has a 0–6% grade. It is well drained and has a Xeric moisture regime.

A (0 – 25 cm): 7.5YR 5/6 strong brown, sandy clay loam. Moderate, fine, subangular blocky structure. Friable, slightly sticky, slightly plastic consistency. Common medium round clasts. Clear, smooth boundary.
Bt (25 – 52cm): 2.5YR 4/6 red, sandy clay. Moderate, medium, subangular blocky structure. Friable, moderately sticky, moderately plastic consistency. Clay films. Many medium clasts with calcic rinds. Wavy, clear boundary.
Bk (52 – 105cm): 10YR 8/3 very pale brown, loamy sand. Common 2.5YR 4/6 red mottles. Strong, medium blocky structure. Firm, non-sticky, non-plastic. Clay and carbonate films. Many course round clasts. Sharp, smooth boundary.
Cr (>105cm): 2.5Y 5/3 light olive brown, silty clay. Common 2.5Y 8/1, white mottles. Strong medium blocky structure. Friable, moderately sticky, moderate plastic consistency. Carbonate and clay films. This

is developed on bedrock below the alluvial terrace in the Miocene to Pliocene, poorly lithified sedimentary rock.

Location: Southwest of Skinias. GPS → N: 35.04875, E: 025.29073. Elevation: 197.7m

Soil developed on a $\mathbf{Q_{t2}}$ alluvial terrace. The upper horizons are matrix-supported, and the lower horizons are clast-supported. Clasts are many and predominantly rounded medium to large limestone with some chert, sandstone, phyllite, and random quartz. The slope is west-facing and has a 0–6% grade. It is well drained and has a Xeric moisture regime.

Ap (0 – 25 cm): 10YR 4/6 light olive brown, sandy loam. Weak, fine, subangular blocky structure. Very friable, slightly sticky, non-plastic consistency. Few pebbles. Smooth, clear boundary.
Bt1 (25 – 65cm): 7.5YR 4/6 strong brown, clay loam. Moderate, medium, subangular blocky structure. Friable, slightly sticky, slightly plastic consistency. Weak clay films. Few pebbles. Gradual, smooth boundary.
Bt2 (65 – 140cm): 2.5YR 4/6 red, clay loam. Moderate, medium, subangular blocky structure. Friable, moderately sticky, slightly plastic consistency. Clay films. Few pebbles. Wavy, clear boundary.
Btk1 (140-168cm): 5YR 4/6 yellowish red, sandy loam. Common 10YR 5/4 yellowish brown mottles. Weak, medium subangular blocky structure. Very friable, slightly sticky, non-plastic. Clay and carbonate films. Common medium round clasts. Clear, wavy boundary.
Btk2 (168-210cm): 5YR 4/4 reddish brown, sandy loam. Moderate medium granular structure. Very friable, slightly sticky, non-plastic. Clay and carbonate films. Common medium round clasts, 0.5 to > 1 mm carbonate rinds on clasts. Clear, smooth boundary.
Cr (>210cm): 2.5Y 5/3 light olive brown, silty clay loam. Common 2.5Y 8/2, pale yellow mottles. Moderate fine blocky structure. Friable, slightly sticky, slightly plastic consistency. Carbonate and clay films. This is developed on bedrock below the alluvial terrace in the Miocene to Pliocene, poorly lithified sedimentary rock.

Location: West of Skinias. GPS → N: 35.063144, E: 025.30551. Elevation: 237.5m

Soil developed on a $\mathbf{Q_{t1}}$ alluvial terrace. The upper horizons are matrix-supported, and the lower horizons are clast-supported. Clasts are many and predominantly rounded medium to large limestone with some chert, sandstone, phyllite, and random quartz. The slope is west-facing and has a 0–6% grade. It is well drained and has a Xeric moisture regime.

A (0 – 25 cm): 5YR 4/6 yellowish-red, sandy clay loam. Weak, fine, subangular blocky structure. Very friable, slightly sticky, non-plastic consistency. Clay films Few pebbles. Smooth wavy boundary

Bt (25 – 63cm): 2.5YR 4/6 red, sandy clay loam. Moderate, medium, subangular blocky structure. Friable, moderately sticky, moderately plastic consistency. Clay films. Common medium to large clasts with >1 mm carbonate rinds. Clear, wavy boundary.
Bk(63-163cm): 5YR 8/1 white, petrocalcic. Extremely strong, medium, subangular blocky structure. Unable to determine consistency because it is petrocalcic. Carbonate films. Many medium to large round clasts, 0.5 to > 1 mm carbonate rinds on clasts. Sharp, smooth boundary.
Cr (>163cm): 2.5Y 7/3 pale yellow, silty clay. Common 2.5Y 8/2, pale yellow mottles. Strong medium blocky structure. Friable, moderately sticky, moderate plastic consistency. Carbonate and clay films. This is developed on bedrock below the alluvial terrace in the Miocene to Pliocene, poorly lithified sedimentary rock.

Location: Northwest of Karavados. GPS → N: 35.06804, E: 025.31046 (R050812-9). Elevation: 237.6m

Soil developed on a $\mathbf{Q_{t3}}$ alluvial terrace. The upper horizons are matrix-supported, and the lower horizons are clast-supported. Clasts are many and predominantly rounded medium to large limestone with some chert, sandstone, phyllite, and random quartz. The slope is south-facing and has a 0–6% grade. It is well drained and has a Xeric moisture regime.

Ap (0 – 20 cm): 2.5Y 6/3 yellowish brown, silty clay loam. Moderate, fine, subangular blocky structure. Friable, slightly sticky, non-plastic consistency. There are a few round clasts. Clear, smooth boundary.
Bt1(20 – 35cm): 7.5Y 5/6 strong brown, sandy clay loam. Moderate, medium, subangular blocky structure. Friable, slightly sticky, slightly plastic consistency. Common round clasts. Clear, smooth boundary.
Bt2 (35 – 105cm): 5YR 4/6 yellowish red, sandy loam. Moderate, fine, subangular block structure. Friable, slightly sticky, non-plastic consistency. Clay films. Many large clasts. Gradual wavy boundary.
BC? Bw? (105-170cm): 10YR 6/4 light yellowish brown, loamy sand. Weak, medium granular structure. Very friable, non-sticky, non-plastic consistency. Many course clasts have thin carbonate rinds (~0.5 mm). Clear, wavy boundary.
Cr (>170cm): 2.5Y 7/3 pale yellow, silty clay. Common 2.5Y 8/2, pale yellow mottles. Strong medium blocky structure. Friable, moderately sticky, moderate plastic consistency. This is developed on bedrock below the alluvial terrace in the Miocene to Pliocene, poorly lithified sedimentary rock.

Location: North of Xoklesi. GPS → N: 35.083288, E: 25.313883. Elevation: 299 m

Soil developed on a $\mathbf{Q_{af3}}$ alluvial fan. The upper horizons are matrix-supported, and the lower horizons are clast-supported. Clasts are many and predominantly rounded medium to large limestone with some chert, sandstone, phyllite, and random quartz. The slope is northeast-facing and has a 0–6% grade. It is well drained and has a Xeric moisture regime.

Ap (0 – 20 cm): 10YR 5/4 yellowish brown, sandy loam. Moderate, medium, subangular blocky structure. Friable, slightly sticky, non-plastic consistency. Few pebbles. Smooth, clear boundary
Bt1 (20 – 65cm): 2.5YR 4/8 red, sandy clay loam. Common 10YR 6/6 yellowish brown mottles. Moderate, medium, subangular blocky structure. Friable, slightly sticky, slightly plastic consistency. Clay films. Few saprolite clasts. Gradual wavy boundary.
Bt2 (65 – 140cm): 2.5YR 4/6 red, sandy clay loam. Common 10YR 7/6 yellow mottles. Strong, medium, blocky structure. Firm, moderately sticky, moderately plastic consistency. Clay films. Few saprolite clasts. Gradual wavy boundary.
Btk (140 – 220cm): 2.5YR 4/6 red, sandy loam. Common 10YR 7/6 yellow mottles. Moderate, medium, blocky structure. Firm, moderately sticky, slightly plastic consistency. Clay and carbonate films. Few saprolite clasts. Gradual wavy boundary.
Btk2 (168-210cm): 5YR 4/4 reddish brown, sandy loam. Moderate medium granular structure. Very friable, slightly sticky, non-plastic. Clay and carbonate films. Common medium round clasts, 0.5 to > 1mm carbonate rinds on clasts. Clear, smooth boundary.
Cr (>210cm): 10YR 5/6 yellowish brown, silty clay loam. Common 5YR 4/6, yellowish-red mottles. Moderate, medium, subangular blocky structure. Very friable, slightly sticky, and slightly plastic consistency. Carbonate and clay films. This is developed on bedrock below the alluvial fan in Miocene to Pliocene, poorly lithified sedimentary rock.